

Tuning the activity and selectivity of polymerised ionic liquids-stabilised ruthenium nanoparticles through anion exchange reactions

Received 18th November 2021,
Accepted 17th February 2022

DOI: [10.1039/D1NR07628K](https://doi.org/10.1039/D1NR07628K)

Dambarudhar Parida,^{a,b} Camille Bakkali-Hassani,^a Eric Lebraud,^c Christophe Schatz,^a Stéphane Grelier,^a Daniel Taton,^a Joan Vignolle^{a*}

ABSTRACT: The development of highly active and selective heterogeneous-based catalysts with tailorable properties is not only a fundamental challenge, but is also crucial in the context of energy savings and sustainable chemistry. Here, we show that ruthenium nanoparticles (RuNPs) stabilised with simple polymerised ionic liquids (PILs) based on N-vinyl imidazolium led to highly active and robust nano-catalysts in hydrogenation reactions, both in water and organic media. Of particular interest, their activity and selectivity could simply be manipulated through counter-anions exchange reactions. Hence, as a proof of concept, the activity of RuNPs could be reversibly turned on and off in the hydrogenation of toluene, while in the case of styrene, the hydrogenation could be selectively switched from ethylbenzene to ethylcyclohexane upon anion metathesis. According to X-Ray photo-electron spectroscopy (XPS) and Dynamic light scattering (DLS) analysis, these effects could originate from the relative hydrophobicity and solvation of the PIL corona but also from the nature and strength of the PIL-Ru interactions.

Introduction

The development of highly active, selective and recyclable catalysts is crucial in the context of energy savings and sustainable chemistry.^{1–7} Metallic nanoparticles (MNPs) are promising candidates because of their unique properties that stem from their nanometric size and the presence of high-energy surface atoms.^{8–13} As MNPs prove thermodynamically unstable respective to bulk metal, stabilisers such as polymers, ligands, surfactants or ionic liquids (ILs) are required to ensure colloidal stability.^{14–18} In addition, stabilisers may also strongly influence the catalytic properties of MNPs, owing to their multiple interaction with the MNPs surface.^{19–25} In this regard, polymeric stabilisers generally lead to highly stable dispersion of MNPs thanks to their steric protection.^{26–29} Meanwhile, steric congestion may limit the access of substrates to the surface, thus decreasing catalytic performances. In contrast, with molecular ILs as stabilisers, very active MNPs are formed.^{30–33} Nevertheless, such dispersions remain poorly stable under forcing conditions,³³ which can be overcome by adding some polymer.³⁴

Polymerised ionic liquids (PILs) are polymeric versions of ionic liquids (ILs), where cations (or anions) are tethered to the polymer backbone and counter-ions are mobile.^{35–39} This class of poly(electrolytes), which combines the properties of polymers with those of ILs, behaves as powerful electro-steric stabilisers for MNPs.^{40–44} Hence, PILs, notably those based on the imidazolium cation, generally lead to PILs-stabilised MNPs catalytic systems, denoted as M@PIL NPs, with enhanced activity and improved stability relative to molecular IL-stabilised MNPs.⁴³ Applications of M@PIL NPs-type catalysts (M = Rh, Pd, Pt, Ni, Au and Ag) have proven efficient in a variety of chemical transformations, including Suzuki,^{45–50} Sonogashira,⁵¹ Heck^{49,50,52} and Stille⁴⁹ C-C couplings, as well as

hydrogenation reactions.^{40,43,44,53–59}

Besides these outstanding stabilising properties, a peculiar advantage of PILs over more conventional stabilisers relies on the facile and reversible tuning of their physical and chemical properties by anion exchange (so-called anion metathesis) reactions. For instance, we have reported that unreactive poly(imidazolium)s could be transformed into reactive PILs thanks to the introduction of basic counter-anions by anion exchange.^{60–62} The resulting poly(imidazolium)s behave as masked poly(N-heterocyclic carbenes) for the purpose of organic catalysis and for post-functionalization as well. Furthermore, the solubility of PILs can be switched from aqueous to organic medium, and *vice versa*, by this simple counter-anions metathesis reaction.^{63,64} By analogy, when coated on MNPs, PILs allow the solubility of M@PIL NPs to be tuned; likewise their reversible transfer from water to an organic solvent has been reported.^{56,65}

As the adsorption of anions on metallic surfaces has been shown to affect the catalytic activity and selectivity of MNPs,^{66–70} we hypothesised that counter-anions exchange reactions could be harnessed to tailor the catalytic properties of PILs-stabilised MNPs (Figure 1 et 2).

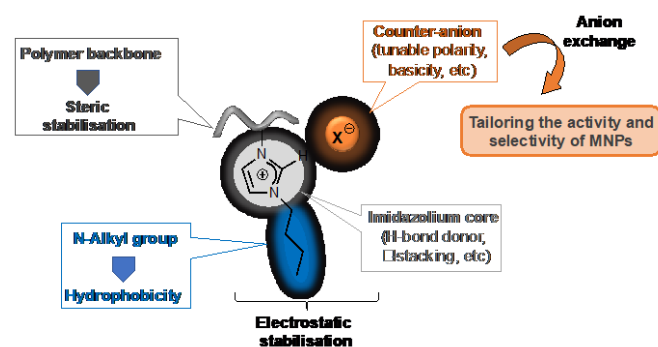


Fig. 1 Features of imidazolium-based PIL to manipulate the catalytic properties of MNPs.

^a Laboratoire de Chimie des Polymères Organiques (LCPO), CNRS, University of Bordeaux, Bordeaux INP, 33600 Pessac, France. Email: joan.vignolle@enscbp.fr

^b Swiss Federal Laboratories for Materials Science and Technology (Empa), St. Gallen, CH-9014, Switzerland

^c University of Bordeaux, CNRS, ICMCB, UMR 5026, F-33600 Pessac, France

Electronic Supplementary Information (ESI) available: Materials. General procedures. Ru content determination by TGA. TEM Analysis of Ru nanoparticles. X-ray diffraction (XRD) patterns of Ru NPs. ζ-potentials of Ru NPs. XPS analysis. Catalytic activity. Activity switching of Ru NPs. References. See DOI: [10.1039/D1NR07628K](https://doi.org/10.1039/D1NR07628K)

We wish to report herein that simple PILs based on poly(1-butyl-3-vinyl imidazolium), associated with different anions, such as Cl, Br, I, bis(trifluoromethyl)sulfonimide (NTf₂) act as very efficient stabiliser for RuNPs both in water and organic media. More importantly, their catalytic activity can be tuned by simple counter-anions exchange reactions (Figure 2). Hence, this effect provides an innovative and powerful means to reversibly turn the catalytic activity of Ru@PIL NPs on and off. Switching the chemo-selectivity of Ru@PIL NPs in the hydrogenation of styrene from ethylbenzene to ethylcyclohexane can also be accomplished upon I[−]/NTf₂[−] anion exchange (Figure 2). On the basis of XPS and DLS analysis, this anion effect could result from the specific interactions between the counter-anions and/or the imidazolium moieties of the PIL stabiliser and the Ru surface, as well as from the relative solvation and hydrophobicity of the PIL corona.

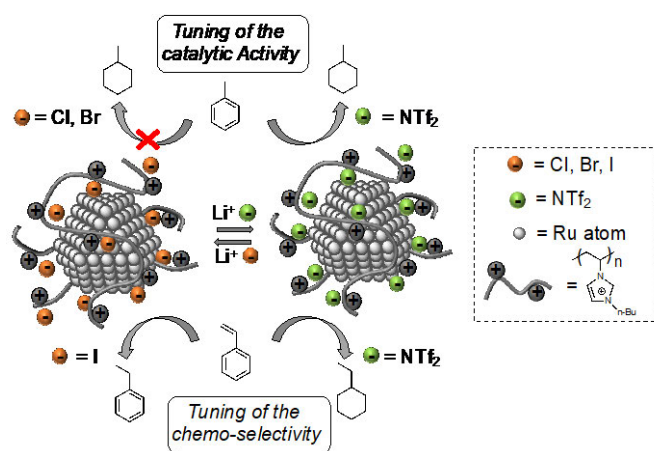


Fig. 2 Tuning the activity and selectivity of polymerised ionic liquid-stabilised Ru nanoparticles by anion exchange. NTf₂ -bis(trifluoromethyl)sulfonimide.

Results and discussion

The ability of poly(1-Butyl-3-vinyl-imidazolium chloride), denoted as PIL(Cl), to stabilise RuNPs was first investigated. PIL(Cl) was prepared by free radical polymerisation of the corresponding N-vinyl imidazolium chloride ionic liquid monomer at 70°C in *iso*-propanol. The corresponding Ru@PIL(Cl) NPs were synthesized by a polyol process (Fig. 3),⁷¹ that is by reduction of RuCl₃ in ethylene glycol at 170 °C, in presence of different amount of PIL(Cl) (for details, see SI).

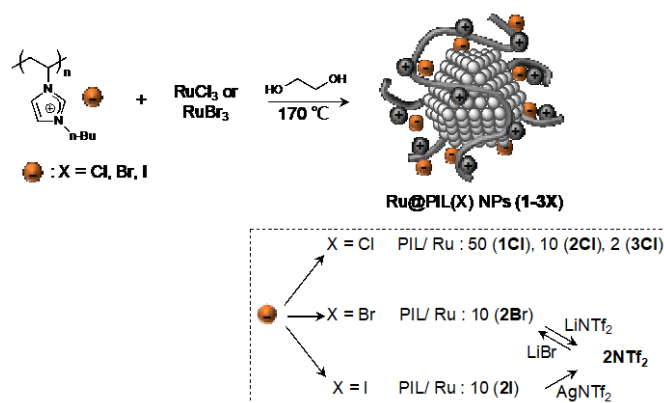


Fig. 3 Preparation of PIL(X)-stabilised RuNPs (1-3X) by polyol process and anion exchange reactions (X = Cl, Br, I, NTf₂).

Using a PIL(Cl)/Ru molar ratio of 50, 10 and 2, mono-disperse NPs of 1.5 nm (**1Cl**), 2.6 nm (**2Cl**) and 2.7 nm (**3Cl**) were formed respectively, according to TEM analysis (Fig. 4). XRD analysis revealed that **1Cl**, **2Cl** and **3Cl** were polycrystalline, the size of the crystalline domains, as determined from the Debye-Scherrer relation, being smaller than the size measured by TEM (1.1 nm, 1.3 nm and 1.4 nm for **1Cl**, **2Cl** and **3Cl** respectively; see Table S4). As an assessment of their stability in water, ζ-potential was then determined. All Ru@PIL(Cl) NPs exhibited positive values as expected from their poly-cationic nature (Fig. 4d). The ζ-potential also increased with the PIL/Ru ratio in the order **3Cl** (35 mV) < **2Cl** (49 mV) < **1Cl** (56 mV), indicating the higher stability of **1Cl**. The Ru(0) and Ru(IV) contents could be evaluated to 88% (BE = 461.4 eV) and 12% (BE = 463.4 eV) by XPS analysis of **2Cl** upon deconvolution of the Ru 3p3/2 signals (Fig. S18, Table S7).

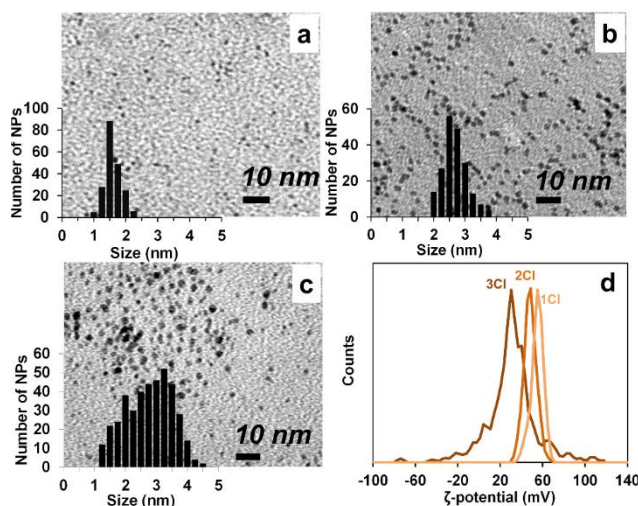
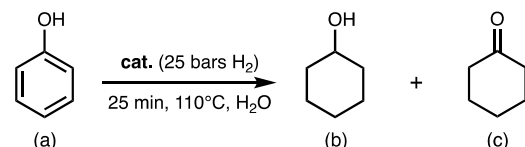


Fig. 4 TEM image and size histogram of (a) **1Cl**, (b) **2Cl**, (c) **3Cl** and (d) Zeta potential of **1-3Cl** in water at 25 °C.

To investigate the influence of the PIL counter-anions on the RuNPs catalytic properties, different Ru@PIL NPs with Br, I and NTf₂ anions were also prepared. **2Br** and **2I** were generated in a similar way as **2Cl**, using PIL(Br) and PIL(I) as stabilisers respectively, with a PIL(X)/Ru ratio equal to 10. In contrast, **2NTf₂** was accessed by anion metathesis between **2Br** and LiNTf₂ because of the insolubility of PIL(NTf₂) in ethylene glycol

(Fig. 2). Importantly, no trace of residual bromide was detected in **2NTf₂** by XPS analysis (Fig. S14 & S15), evidencing that the anion exchange was quantitative. Alternatively, **2Cl** could be used instead of **2Br** for the anion metathesis, the anion exchange being also complete in this case (Fig. S15b). The size of the RuNPs was not affected by the anion exchange reaction but was found to decrease in the order: **2Cl** (2.6 nm) > **2Br/2NTf₂** (2.3 nm) > **2I** (1.6 nm) according to TEM analysis, highlighting the influence of the PIL counter-anions over the NPs size (Fig. S5 and S6). Although the origin of this effect is not clearly understood, it may result from the nature and intensity of the PIL/Ru and cation/anion interactions (*vide infra*).

Table 1. Hydrogenation of phenol in water catalysed by RuNPs.

			
Entry	NP	Conversion (%)	Selectivity (b %)
1	1Cl	62	88
2	2Cl	100	100
3	3Cl	100*	100
4	2Br	100	100
5 ^a	Ru@IL	100*	100
6 ^b	Ru@PVP	100*	100

Hydrogenation were performed with 0.166 mol.% of Ru catalyst and 6 wt% of phenol in 5 mL of water, at 110 °C, under 25 bars of H₂. The conversion was determined by ¹H NMR. The selectivity was confirmed by GC-MS analysis.

*Aggregation of NPs and/or bulk metal formation was observed. ^aIL: 1-butyl-3-ethyl-imidazolium bromide. ^bSee SI for their preparation and characterization.

Hydrogenation of phenol with Ru@PIL(X) NPs in water (X = Cl, Br)

The catalytic activity of **1-3Cl** was first investigated for the hydrogenation of phenol in water as model reaction (Table 1).⁷² Reactions were performed at 110 °C for 25 min, using 25 bars of H₂ and 0.166 mol.% of Ru loading. Under those conditions, **2Cl** appeared as the most efficient catalyst, providing full substrate conversion, as well as complete selectivity in favour of cyclohexanol (entry 2). In comparison, **1Cl** and **3Cl** displayed a moderate conversion (62 %, entry 1) and a poor stability (entry 3), respectively, highlighting that an intermediate ratio PIL/Ru ratio of 10 was the optimal balance. The same ratio was thus kept throughout the study. The formal replacing of Cl⁻ by Br⁻ had virtually no influence on the catalytic properties of such Ru@PIL(X) systems, as indicated by the full substrate conversion and full selectivity toward cyclohexanol obtained with **2Br**, under similar conditions (entry 4). For comparison purpose, RuNPs either electrostatically stabilised by an homologous monomeric ionic liquid, namely, 1-Butyl-3-ethylimidazolium bromide, or sterically stabilised with neutral PVP were prepared by the same polyol process (see part 2b in SI), yielding to water-dispersible RuNPs of 1.8 and 2.7 nm respectively. In both cases, aggregation of the NPs and bulk metal formation were observed (Table 1, entry 5 and 6) under the standard

conditions (110 °C, 25 min, 25 bars of H₂). In contrast, **2Br** and **2Cl** remained perfectly stable.

The recyclability of Ru@PIL NPs was also briefly examined. Quantitative phenol conversion could thus be achieved over 7 cycles with **2Cl**, without any sign of NP aggregation according to TEM analysis (Fig. S24 & S25). Although hydrogenation of aromatics generally involves heterogeneous species as catalysts, a CS₂ poisoning experiment was performed to confirm the heterogeneous nature of the catalyst.⁷³ Thus, upon addition of CS₂ to the catalytic solution containing **2Cl**, no further increase of the conversion with time was noted (Fig. S26), in agreement with a surface-mediated catalysis.

Switching of the catalytic activity by anion exchange

As Ru@PIL(X)NPs (**2Cl**, **2Br**, **2NTf₂** and **2I**) display different solubility depending on the type of counter-anions introduced, methanol was selected as common solvent to compare their catalytic activity under semi-heterogeneous conditions. Hydrogenation reactions were performed at 110 °C for 1 h, using 25 bars of H₂ and phenol as substrate. Under those conditions, **2I** proved completely inactive, while **2Br**, **2Cl** and **2NTf₂** afforded low substrate conversion of 2, 6 and 11% respectively (Table 2).

Table 2. Influence of PIL counter-anions over the catalytic activity of Ru@PIL(X) NPs (X = Cl, Br, I, NTf₂) for the hydrogenation of phenol and toluene.

Entry	NP	Phenol Conversion (%)	Toluene Conversion (%)
1	2Cl	6	10
2	2Br	2	2
3	2I	0	0
4 ^a	2NTf ₂	11	70
5 ^b	2Br ^l	-	5

Hydrogenation of phenol and toluene (6 wt% in 5 mL of methanol) were performed at 110 °C for 60 min using 0.33 mol.% of Ru catalyst and 25 bars of H₂. In all cases, conversion was determined by GC-MS. ^a2NTf₂ was prepared by anion exchange of **2Br** with LiNTf₂. ^b2Br^l was prepared by anion exchange of **2NTf₂** with LiBr.

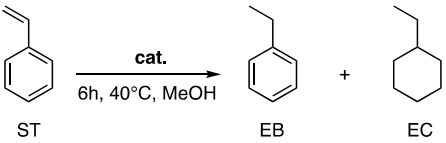
Although higher conversion was observed upon Br/NTf₂ anion exchange (2 and 11% for **2Br** and **2NTf₂** respectively, see entries 2 and 4), phenol conversion remained very low regardless of the catalyst. Toluene was next tested to evaluate the influence of the PIL counter-anions in the case of hydrophobic substrates. Here again, under the same experimental conditions, **2I** proved completely inactive, while **2Cl** and **2Br** afforded 10 and 2% of methylcyclohexane respectively (Table 2). To our delight, **2NTf₂**, resulting from a Br/NTf₂ anion exchange, provided 70% of conversion. Thus, the simple replacement of the hydrophilic bromide by the hydrophobic and weakly coordinating NTf₂ anion allowed the catalytic activity to be dramatically increased in the case of toluene. Remarkably, this process is reversible as the addition of LiBr to **2NTf₂** turned the catalyst back to its inactive form **2Br^l** (conv. ~ 5%) (Fig. S27). However, in contrast to the Br⁻/NTf₂⁻ anion exchange, 8% of NTf₂⁻ remained in **2Br^l** according to XPS analysis (Figure S17), highlighting that the exchange was

incomplete in this case. Thus, the catalytic activity of Ru@PIL(X) NPs could be switched on and off thanks to the reversible exchange of the PIL counter-anions. Although the influence of some anions over the catalytic properties of MNPs has been reported,⁶⁹ this anion exchange-mediated reversible switching of the catalytic activity is unprecedented to the best of our knowledge. This reversible behaviour originates from the specific properties of the PIL stabilisers, which combine a macromolecular structure and multiple, relatively weak anion-cation interactions. As already reported for other MNPs, this anion exchange reaction also allows the polarity of the catalysts to be readily modified (Table S2),^{56,65} leading to quantitative hydrogenation of toluene with **2NTf₂** as catalyst in THF as solvent (Table S10).

Switching of the catalytic selectivity by anion exchange

The inability of **2I** to hydrogenate aromatics (Table 2), prompted us to investigate the selective hydrogenation of C=C bonds using styrene as model substrate (Table 3). Thus, hydrogenation of styrene was performed at 40 °C under 15 bars of H₂, in presence of a catalytic amount of **2I** (0.33 mol% of Ru). Under these conditions, we were pleased to observe full substrate conversion and complete selectivity for ethylbenzene (EB) (Table 3, entry 2).

Table 3. Hydrogenation of styrene (ST) to ethylbenzene (EB) and ethylcyclohexane (EC) using Ru@PIL(X) NPs (X = Br, I, NTf₂) as catalysts.

			
Entry	NP	Conversion (%)	EB/EC selectivity (%)
1	2Br	100	64/36
2	2I	100	100/0
3	2NTf ₂ ^a	100	0/100
4	Ru/C (5%) ^b	100	16/84

Hydrogenation in methanol (5 ml methanol and 6 wt% of styrene) at 40 °C for 6 hours under 15 bar of H₂ and 0.33 mol.% of Ru loading. GC-MS was used to determine conversion and chemo-selectivity of different catalysts. ^a2NTf₂ was prepared by anion exchange between 2I and AgNTf₂. ^bCommercial catalyst.

In the case of **2Br**, styrene was fully converted into a mixture of 64% of EB and 36% of ethylcyclohexane (EC), highlighting a lack of chemo-selectivity in this case. In sharp contrast, when **2NTf₂** was used under identical conditions, both the vinyl group and the aromatic ring were quantitatively reduced (entry 3). Interestingly, **2NTf₂** could be generated from **2I** using AgNTf₂ (SI Sec. 2c), which enabled the chemo-selective hydrogenation of styrene to be switched from EB to EC, upon I[−]/NTf₂[−] anion exchange, while maintaining quantitative conversion (Fig. S16). For comparison, hydrogenation of styrene was also performed with Ru/C (5%) under the same conditions, leading to a mixture of EB (16%) and EC (84%) (Entry 4), and thus evidencing the superior selectivity of Ru@PIL(X) NPs. Overall, those results not only demonstrated

the interest of Ru@PIL(X) NPs catalytic systems relative to commercial catalysts, but also further highlighted the influence of PIL counter-anions over the catalytic properties.

Investigation of the PIL(X)-RuNPs interactions in the solid state

To gain more insight into the influence of the nature of PILs on NP properties, XPS analysis was performed on all Ru@PIL(X) NPs, *i.e.* **2Cl**, **2Br**, **2I** and **2NTf₂** (prepared from **2Br** by anion exchange), as well as on corresponding PIL(X) stabilisers (X = Cl, Br, I, NTf₂; Fig.5). Although this analysis is performed in the solid state, it provides qualitative information on the nature and relative strength of PIL-Ru interactions.

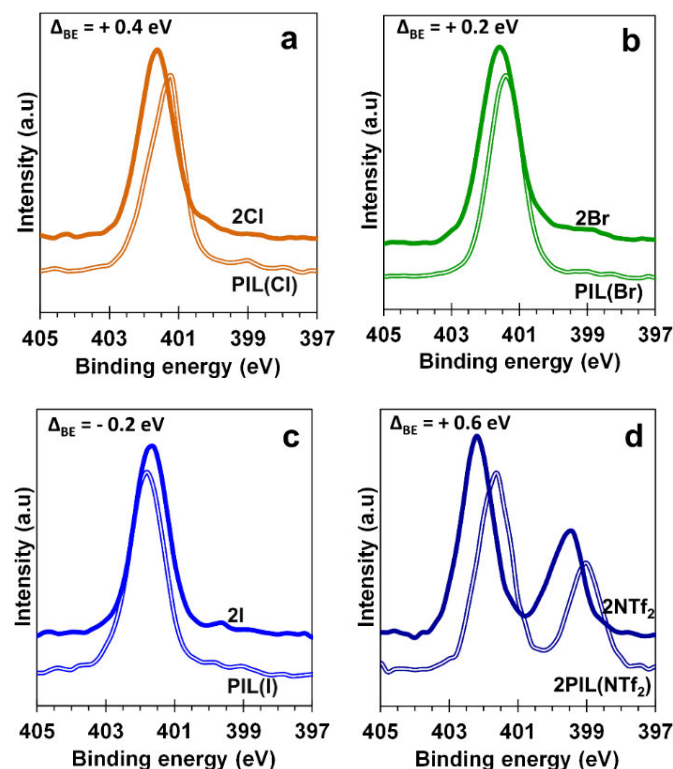


Fig. 5 Overlay of high resolution XPS scans in N(1s) region showing (a) PIL(Cl) and **2Cl**, (b) PIL(Br) and **2Br**, (c) PIL(I) and **2I** (d) PIL(NTf₂) and **2NTf₂**.

Except iodide (I[−]), all anions were found to interact with the Ru surface as evidenced by the shift toward higher binding energy (BE) of the signals associated to Cl(2p), Br(3p), N(1s)NTf₂ compared to their respective BE in the free polymer (Fig. S21). More specifically, the strongest interaction with the Ru surface was observed for both Br and NTf₂ anions ($\Delta BE = +0.4$). In the case of I[−], no detectable shift in the BE I(3d) was observed between PIL(I) and the corresponding RuNPs **2I**, suggesting the absence of interaction between I[−] and the Ru surface.

The environment around the imidazolium cation was next scrutinized by analysing the BE of the N(1s)Im. In the free PIL(X), anions interact solely with imidazolium cations, likely by H-bonding with the C₂-H and C_{4,5}-H.⁷⁴ The BE N(1s)Im was found to increase with an increase of the polarizability of the anion in the order: Cl (401.2 eV) < Br (401.4 eV) < NTf₂ (401.6 eV) < I (401.8 eV) (Fig. 5a-d and Table S8). Thus, the most polarizable NTf₂[−] and I[−] anions only weakly interact with the

imidazolium cation, leading to a cationic structure, where the electrons are tightly bound to the N atom. In contrast, the low BE N(1s)Im observed for Cl reflects its strong interaction with the imidazolium moiety via H-bonding, which virtually led to a partial transfer of the positive charge from the nitrogen atom to the proton.

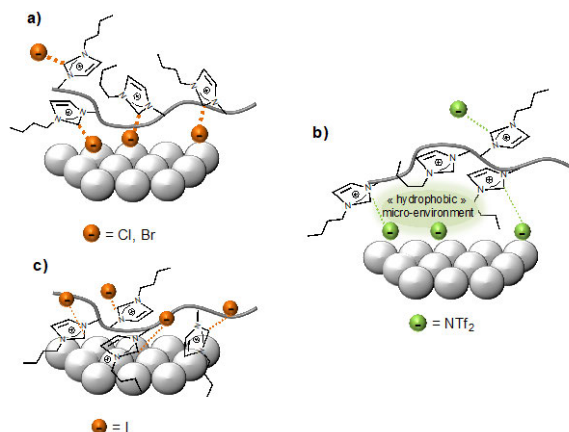


Fig.6 Schematic representation of the interaction between PIL(X) and the Ru surface with (a) PIL(X=Cl or Br), (b) PIL(NTf₂) and (c) PIL(I).

In Ru@PIL(X) NPs (X= Cl, Br and NTf₂), the signal corresponding to N(1s)Im was shifted to higher BE relative to that of their respective PIL(X), indicating a weakening of the anion-cation interactions in presence of Ru. This effect was more pronounced for 2NTf₂ ($\Delta_{BE} = +0.6$) than for 2Cl ($\Delta_{BE} = +0.4$) and 2Br ($\Delta_{BE} = +0.2$) (Fig. 5a, b and d and fig. 6a,b). In sharp contrast, a 0.2 eV shift toward lower BE was noted for the N(1s)Im of 2I, relative to that of PIL(I) (Fig. 5c), suggesting an interaction between imidazolium cations and the Ru surface (Fig. 6c).^{75,76} From a catalysis point of view, such interactions would prevent aromatic substrates from adsorbing onto the flat surface of faces and to undergo hydrogenation of the aromatic moiety (fig. S23), as observed experimentally with 2I and toluene and styrene as substrates. However, binding of styrene *via* the alkene moiety to edges or corners of RuNPs would not be hindered,^{8,77,78} allowing for complete EB selectivity with 2I as catalyst. Note also that the smaller size of 2I relative to 2Cl and 2Br observed by TEM (Fig. S5) may also originate from this peculiar imidazolium-Ru interaction, which would inhibit NP growth during their synthesis.

Influence of the PIL counter-anions (X) over the properties of Ru@PIL(X) NPs in solution

Dynamic light scattering (DLS) was performed on 2Br, 2NTf₂ and 2I in MeOH in order to investigate the influence of the counter-anions over the solution properties of NPs. The intensity-weighted size distributions were found to be bimodal for 2Br and 2NTf₂, suggesting the presence of some aggregation that likely resulted from inter-particular hydrogen bonding between imidazolium cations and respective counter-anions (fig. 7a).⁷⁴ However, the number-weighted size distributions of 2Br and 2NTf₂ indicated that the proportion of these aggregates was very small, a single population at 8 and

12 nm, corresponding to isolated NPs, being observed for 2Br and 2NTf₂ respectively (fig. 7b).

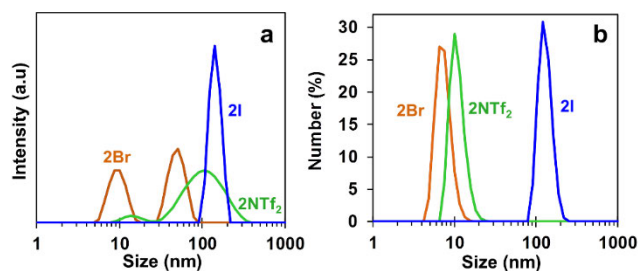


Fig.7. DLS of 2Br, 2NTf₂ and 2I shown in (a) intensity-weighted size distributions and (b) number-weighted size distributions.

In contrast, only aggregates of about 180 nm were observed for 2I on both types of size distribution (fig. 6a, b), which could result from the peculiar binding mode of PIL(I) to Ru that involves interactions between the poly(cationic) chains and the Ru surface, as demonstrated by XPS analysis (fig. 6c).

All these data clearly evidenced that the nature of PILs counter-anions has a dramatic impact on the nature and strength of the PIL-Ru and anion-cation interactions, both in the solid state and in solution. While the selectivity observed with 2I could originate from the peculiar imidazolium-Ru interaction, the higher activity of 2NTf₂, relative to 2Br, in the hydrogenation of toluene and styrene could be ascribed to a more favourable micro-environment due to the better solvation of the PIL corona on one hand (Fig. 7b), and, on the other hand, to the relative hydrophobicity due to the presence of *n*-butyl substituents on imidazolium units and NTf₂⁻ counter-anions (Fig. 6b).

Conclusions

Easily accessible imidazolium-based polymerised ionic liquids (PILs) behave as powerful electro-steric stabilisers for RuNPs, affording highly active systems for the hydrogenation of aromatic substrates in different solvents such as water, MeOH or THF. In comparison to more conventional stabilisers, PILs provide a tailorable micro-environment around the metallic surface, which enable for reversibly controlling the catalytic properties of the corresponding RuNPs by simple exchange of the PIL counter-anions. Hence, this strategy allows, not only the catalytic activity to be turned on and off, but also the chemo-selectivity of RuNPs to be switched depending on the nature of the counter-anions. According to XPS and DLS analysis, influence of the PIL over the activity and selectivity of RuNPs stems from the relative hydrophobicity and solvation of the PIL corona and from the nature (via the anion or the cation) and strength of PIL-Ru interactions, respectively. Overall, this work demonstrates that, conceptually, different activity and selectivity can be reached from a single catalyst through anion exchange reactions. The variety of cations and anions available offers a bright horizon to tailor the metal surface properties of MNPs, via simple anionic metathesis. Future work is underway to extend this concept to other

poly(electrolyte)s and other metals, for a wide range of transformations.

Experimental and methods

Preparation of poly(ionic liquid)s (PILs) and Ru@PIL(X) NPs

Polymerised ionic liquids PIL(X) (X = Cl, Br, I) were prepared by free radical polymerisation of the corresponding 1-butyl-3-vinyl-imidazolium ionic liquid (ILs) monomers at 70 °C for 24 h, using AIBN as initiator (IL/AIBN = 200). ¹H NMR analysis after polymerisation confirmed 100% conversion of IL(Cl) and IL(Br). Conversion of 75% was obtained in the case of IL(I) after 48 hours of polymerisation. Poly(1-Butyl-3-vinylimidazolium chloride) (PIL(Cl)) and Poly(1-Butyl-3-vinylimidazolium bromide) (PIL(Br)) were precipitated repeatedly in diethyl ether and dried under vacuum (35 °C) till a constant weight was obtained (quantitative yields). PIL(I) was precipitated once in diethyl ether and then taken for dialysis against methanol to remove the remaining IL(I) monomer. After 48 hours of dialysis, PIL(I) was collected by precipitation in diethyl ether and dried under vacuum (35 °C) till a constant weight was obtained with a final yield of 60%. All PIL(X) (X = Cl, Br, I) were analysed by ¹H NMR to confirm the absence of any residual monomer (Fig. S1). Macromolecular characteristics of the PILs were determined by size exclusion chromatography (SEC) (table S1). Prior to SEC analysis, all PILs were converted to PIL(NTf₂) by anion exchange to make them soluble in the mobile phase (THF) (SI, sec. 2a).

PIL(X)-stabilised RuNPs (Ru@PIL(X) NPs) (X = Cl, Br & I) were prepared using RuCl₃·xH₂O and RuBr₃·xH₂O as metal precursors and PIL(Cl), PIL(Br) or PIL(I) as stabilisers via polyol process. Different molar ratio between PIL(X) (repeating IL(X) units) to metal salt (*i.e.* 50:1, 10:1, 2:1) were used to synthesise Ru@PIL NPs.

Typically, 400 mg of PIL(X = Cl, Br & I) and required quantity of metal salt were dissolved in 40 ml ethylene glycol in a 200 ml Schlenk flask. After stirring for 4 hours at 750 rpm, the resulting dark yellow solution was degassed with argon and immersed in an oil bath pre-heated at 170 °C. The dark yellow solution slowly turned black, indicating the formation of Ru(0)NPs. Heating was continued for 1.5 hours to ensure complete conversion of ruthenium salt to Ru(0). Complete reduction of Ru(+2) salts and formation of NPs was confirmed by UV-vis spectroscopy analysis (see SI). Disappearance of the broad absorption band in the spectrum of the precursor after reduction indicates complete reduction of Ru(+2) into Ru(0). A representative example is given in Fig. S1 with the reduction of RuCl₃ in presence of PIL(Cl). PILs stabilised NPs were collected by centrifuging 5 ml of NP solution with 30 ml mixture of diethyl ether and acetone (50:50). After this initial centrifugation, RuNPs were dissolved in acetone (15 mL) and diethyl ether was added (20 mL); the resulting suspension was then subjected to centrifugation. This step was repeated once. The resulting sticky black product was next dissolved in 5 mL of methanol and centrifuged with 25 mL of diethyl ether. The resulting shiny black product was vacuum dried at 35 °C (0.8

mmHg) till a constant weight was obtained (24 - 48h). This step ensures the removing of the different solvents, including ethylene glycol (b.p. = 197 °C). All centrifugations were carried out at 8000 rpm for 15 min at 15 °C. The resulting shiny black products **1Cl** (PIL(Cl)/Ru = 50), **2Cl** (PIL(Cl)/Ru = 10), **3Cl** (PIL(Cl)/Ru = 2), **2Br** (PIL(Br)/Ru = 10) and **2I** (PIL(I)/Ru = 10) were vacuum dried at 35 °C till a constant weight was obtained.

To obtain hydrophobic Ru@PIL(NTf₂) NPs, *i.e.* **2NTf₂**, a Br⁻ / NTf₂⁻ anion exchange was performed from **2Br**. In a typical anion exchange procedure, 10 ml aqueous solution of LiNTf₂ (4 molar equivalent) was added dropwise to 30 ml aqueous solution (1.5 mg/ml) of **2Br** under vigorous stirring, leading to the slow precipitation of **2NTf₂**. To ensure complete exchange, the mixture was stirred for 16 hours under ambient temperature. All operations were carried out under argon atmosphere. Resulting precipitates were washed several times with water and then dried under vacuum at 35 °C until a constant weight was obtained. The solubility of the different RuNPs was examined in a variety of solvents (Table S2). Alternatively, **2NTf₂** could be prepared from **2Cl**, following the same procedure. The reverse process, involving NTf₂⁻ / Br⁻ anion exchange, could also be performed on **2NTf₂**. In a typical procedure, excess of LiBr (4 molar equivalent) pre-dissolved in acetone was added dropwise to **2NTf₂** solution in acetone (1.5 mg/ml) and stirred overnight under inert atmosphere. Upon anion exchange, **2Br'** precipitated out of the solution. Removal of excess LiBr was accomplished by washing the precipitate with acetone. **2I** could also undergo a complete I⁻ / NTf₂⁻ anion exchange by using AgNTf₂ as the source of NTf₂⁻. Here, methanol was used as the solvent during anion exchange and AgI was obtained as the solid precipitate. AgI was removed by centrifugation to obtain a solution of **2NTf₂**, which was then evaporated under vacuum to obtain **2NTf₂** (SI, sec. 2c).

Characterizations of nanoparticles

Ru content of all NP samples was determined by thermo gravimetric analysis (TGA) using a TGA Q-500 from TA instruments. TGA was performed in two steps: in the first step, samples were heated till 600 °C under nitrogen to remove PILs. In the next step, air was introduced after 600 °C to facilitate removal of residual char by combustion. The residual weight obtained around 615 °C was considered as the Ru content as all carbon-based matter had been removed.

Particle sizes of RuNPs were determined by recording Transmission electron microscopic (TEM) image by Hitachi 7650 TEM operating at 80 kV in high-resolution mode. Samples for TEM analyses were prepared by putting a drop of NP solution (0.5 mg/ml in methanol) on a carbon coated copper grid and drying it for 90 minutes before analysis. Particle size and distribution were determined by measuring 200 particles at random locations by Image J software.

XRD patterns were recorded on a PANalytical X'pert MPD-PRO Bragg-Brentano θ - θ geometry diffractometer equipped with a secondary monochromator and an X'celerator detector

over an angular range of $2\theta = 20\text{--}80^\circ$. The Cu-K α radiation was generated at 45 kV and 40 mA ($\lambda = 0.15418\text{ nm}$).

Particle size and ζ -potentials of NPs were determined by dynamic light scattering at 25°C at a concentration of 0.5 mg/ml using Malvern Zetasizer ZS equipment. All the particle size analysis was carried out using methanol as the solvent. ζ -potentials were measured using folded capillary cells (DTS 1070). Based on the solubility, both water and methanol were used as solvent.

X-ray photoelectron spectroscopy (XPS) analysis was carried out in a K-Alpha X-ray Photoelectron Spectrometer from Thermo Fisher Scientific equipped with monochromatized AlK α source ($h\nu = 1486.6\text{ eV}$). The full spectra ($0\text{--}1350\text{ eV}$) and high-resolution spectra were recorded with constant pass energy of 200 eV and 40 eV respectively. Ar⁺ sputtering was used for depth profiles and high-resolution spectra were processed with AVANTAGE software. All scans were corrected considering C(1s) as the reference (285.0 eV).

Hydrogenation procedure

Hydrogenation of unsaturated hydrocarbons was carried out in high pressure Parr reactor with internal volume of 45 ml and equipped with two valves, a manometer and a magnetic stirrer. In a typical hydrogenation, 5 ml of solvent were taken in a Schlenk to which 6 wt\% of substrate and required quantity of NP catalyst were added. In the first method, solution of substrate and catalyst were charged into the reactor and the reactor was flushed three times with H_2 prior to sealing it with desired pressure. Then the reactor was immersed in the oil bath at the set temperature and reaction start time was noted when stirring speed reached 1000 rpm . Reaction was stopped by cooling the reactor by liquid nitrogen and releasing the H_2 pressure. In the second method of hydrogenation (preconditioning route), solution of substrate and catalyst was preheated to reaction temperature prior to flushing and sealing it with desired H_2 pressure. ^1H NMR analysis was used to determine conversion of substrate. In case of phenol hydrogenation, diethyl ether was used to extract the product and after evaporating diethyl ether at room temperature (15 min), product was analysed by ^1H NMR. When organic solvents were used as a solvent for hydrogenation, aliquots were diluted with deuterated solvents for ^1H NMR analysis.

Conversion and selectivity of some hydrogenation reactions were also determined by a Thermo Scientific GC-MS with Trace Ultra GC and Trace DSQ MS. Instrument was equipped with a RESTEK Rtx-5 Sil MS column ($0.25\text{ mm} \times 30\text{ m}$) and helium (0.8 ml/min) was used as the carrier gas.

Catalyst recycling

NP recycling for hydrogenation was carried out with 2Cl using phenol as a substrate. After 25 min . of hydrogenation, product was extracted with diethyl ether. Then, required quantity of phenol was added to the NP solution and reactor was closed and was flushed thrice with H_2 before sealing it at a desired pressure. Reactor was immersed in an oil bath at required temperature and start time was noted when stirring speed

reached 1000 rpm . After completion of hydrogenation, the same procedure was repeated for the next cycle.

Conflicts of interest

There are no conflicts to declare.

Acknowledgements

The authors are grateful to CNRS and to the Agence Nationale de la Recherche (ANR), ANR JCJC (CATAPILS Project ANR-14-CE05-0027-01) for financial support. We are extremely thankful to Christine Labrugere-Sarroste of PLACAMAT UMS-3626 for XPS analysis and helpful discussions. Dr Olivier Sandre is warmly acknowledged for his help on fitting XRD data. We extend special thanks to Bordeaux Imaging Center for TEM analysis.

Notes and References

- 1 F. Zaera, *Coord. Chem. Rev.*, 2021, **448**, 214179.
- 2 L. Zhang, M. Zhou, A. Wang and T. Zhang, *Chem. Rev.*, 2020, **120**, 683–733.
- 3 M. K. Samantaray, E. Pump, A. Bendjeriou-Sedjerari, V. D'Elia, J. D. A. Pelletier, M. Guidotti, R. Psaro and J.-M. Basset, *Chem. Soc. Rev.*, 2018, **47**, 8403–8437.
- 4 R. Ye, T. J. Hurlburt, K. Sabyrov, S. Alayoglu and G. A. Somorjai, *Proc. Natl. Acad. Sci.*, 2016, **113**, 5159–5166.
- 5 M. Sankar, N. Dimitratos, P. J. Miedziak, P. P. Wells, C. J. Kiely and G. J. Hutchings, *Chem. Soc. Rev.*, 2012, **41**, 8099–8139.
- 6 G. A. Somorjai and R. M. Rioux, *Catal. Today*, 2005, **100**, 201–215.
- 7 A. T. Bell, *Science*, 2003, **299**, 1688–1691.
- 8 G. Schmid, *Nanoparticles: From Theory to Application*, John Wiley & Sons, 2011.
- 9 L. Liu and A. Corma, *Chem. Rev.*, 2018, **118**, 4981–5079.
- 10 Y. Du, H. Sheng, D. Astruc and M. Zhu, *Chem. Rev.*, 2020, **120**, 526–622.
- 11 M. Zahmakiran and S. Özkar, *Nanoscale*, 2011, **3**, 3462–3481.
- 12 H. Bönemann and R. M. Richards, *Eur. J. Inorg. Chem.*, 2001, **2001**, 2455–2480.
- 13 A. Roucoux, J. Schulz and H. Patin, *Chem. Rev.*, 2002, **102**, 3757–3778.
- 14 J. D. Aiken and R. G. Finke, *J. Mol. Catal. Chem.*, 1999, **145**, 1–44.
- 15 L. S. Ott and R. G. Finke, *Coord. Chem. Rev.*, 2007, **251**, 1075–1100.
- 16 J. Dupont and J. D. Scholten, *Chem. Soc. Rev.*, 2010, **39**, 1780–1804.
- 17 N. Toshima and T. Yonezawa, *New J. Chem.*, 1998, **22**, 1179–1201.
- 18 D. Astruc, F. Lu and J. R. Aranzaes, *Angew. Chem. Int. Ed.*, 2005, **44**, 7852–7872.
- 19 T. Chen and V. O. Rodionov, *ACS Catal.*, 2016, **6**, 4025–4033.
- 20 P. Lara, K. Philippot and B. Chaudret, *ChemCatChem*, 2013, **5**, 28–45.
- 21 L. Lu, S. Zou and B. Fang, *ACS Catal.*, 2021, **11**, 6020–6058.
- 22 C. A. Schoenbaum, D. K. Schwartz and J. W. Medlin, *Acc. Chem. Res.*, 2014, **47**, 1438–1445.
- 23 P. Liu, R. Qin, G. Fu and N. Zheng, *J. Am. Chem. Soc.*, 2017, **139**, 2122–2131.
- 24 A. Heuer-Jungemann, N. Feliu, I. Bakaimi, M. Hamaly, A.

- Alkilany, I. Chakraborty, A. Masood, M. F. Casula, A. Kostopoulou, E. Oh, K. Susumu, M. H. Stewart, I. L. Medintz, E. Stratakis, W. J. Parak and A. G. Kanaras, *Chem. Rev.*, 2019, **119**, 4819–4880.
- 25 S. G. Kwon, G. Krylova, A. Sumer, M. M. Schwartz, E. E. Bunel, C. L. Marshall, S. Chattopadhyay, B. Lee, J. Jellinek and E. V. Shevchenko, *Nano Lett.*, 2012, **12**, 5382–5388.
- 26 A. Gual, C. Godard, S. Castillón and C. Claver, *Dalton Trans.*, 2010, **39**, 11499–11512.
- 27 L. S. Ott, B. J. Hornstein and R. G. Finke, *Langmuir*, 2006, **22**, 9357–9367.
- 28 A. S. Dunn, *Br. Polym. J.*, 1986, **18**, 278–278.
- 29 Z. B. Shifrina, V. G. Matveeva and L. M. Bronstein, *Chem. Rev.*, 2020, **120**, 1350–1396.
- 30 J. Dupont, G. S. Fonseca, A. P. Umpierre, P. F. P. Fichtner and S. R. Teixeira, *J. Am. Chem. Soc.*, 2002, **124**, 4228–4229.
- 31 K. L. Luska, P. Migowski and W. Leitner, *Green Chem.*, 2015, **17**, 3195–3206.
- 32 C. Vollmer and C. Janiak, *Coord. Chem. Rev.*, 2011, **255**, 2039–2057.
- 33 G. S. Fonseca, A. P. Umpierre, P. F. P. Fichtner, S. R. Teixeira and J. Dupont, *Chem. – Eur. J.*, 2003, **9**, 3263–3269.
- 34 P. Migowski and J. Dupont, *Chem. – Eur. J.*, 2007, **13**, 32–39.
- 35 W. Qian, J. Texter and F. Yan, *Chem. Soc. Rev.*, 2017, **46**, 1124–1159.
- 36 D. Mecerreyes, *Prog. Polym. Sci.*, 2011, **36**, 1629–1648.
- 37 J. Yuan and M. Antonietti, *Polymer*, 2011, **52**, 1469–1482.
- 38 J. Yuan, D. Mecerreyes and M. Antonietti, *Prog. Polym. Sci.*, 2013, **38**, 1009–1036.
- 39 A. Eftekhari and T. Saito, *Eur. Polym. J.*, 2017, **90**, 245–272.
- 40 S. Bulut, Z. Fei, S. Siankevich, J. Zhang, N. Yan and P. J. Dyson, *Catal. Today*, 2015, **247**, 96–103.
- 41 K. Manojkumar, A. Sivaramakrishna and K. Vijayakrishna, *J. Nanoparticle Res.*, 2016, **18**, 103.
- 42 J.-K. Sun, Z. Kochovski, W.-Y. Zhang, H. Kirmse, Y. Lu, M. Antonietti and J. Yuan, *J. Am. Chem. Soc.*, 2017, **139**, 8971–8976.
- 43 X. Mu, J. Meng, Z.-C. Li and Y. Kou, *J. Am. Chem. Soc.*, 2005, **127**, 9694–9695.
- 44 S. Prescher, F. Polzer, Y. Yang, M. Siebenbürger, M. Ballauff and J. Yuan, *J. Am. Chem. Soc.*, 2014, **136**, 12–15.
- 45 Y. Gu, I. Favier, C. Pradel, D. L. Gin, J.-F. Lahitte, R. D. Noble, M. Gómez and J.-C. Remigy, *J. Membr. Sci.*, 2015, **492**, 331–339.
- 46 J. Wang, G. Song and Y. Peng, *Tetrahedron Lett.*, 2011, **52**, 1477–1480.
- 47 N. Jiao, Z. Li, Y. Wang, J. Liu and C. Xia, *RSC Adv.*, 2015, **5**, 26913–26922.
- 48 S. Doherty, J. G. Knight, T. Backhouse, E. Abood, H. Al-shaikh, A. R. Clemmet, J. R. Ellison, R. A. Bourne, T. W. Chamberlain, R. Stones, N. J. Warren, I. J. S. Fairlamb and K. R. J. Lovelock, *Adv. Synth. Catal.*, 2018, **360**, 3716–3731.
- 49 X. Yang, Z. Fei, D. Zhao, W. H. Ang, Y. Li and P. J. Dyson, *Inorg. Chem.*, 2008, **47**, 3292–3297.
- 50 S. Ghasemi and Z. A. Harandi, *RSC Adv.*, 2018, **8**, 14570–14578.
- 51 Y. Wang, J. Liu and C. Xia, *Tetrahedron Lett.*, 2011, **52**, 1587–1591.
- 52 K. Qiao, R. Sugimura, Q. Bao, D. Tomida and C. Yokoyama, *Catal. Commun.*, 2008, **9**, 2470–2474.
- 53 S. Montolio, C. Vicent, V. Aseyev, I. Alfonso, M. I. Burguete, H. Tenhu, E. García-Verdugo and S. V. Luis, *ACS Catal.*, 2016, **6**, 7230–7237.
- 54 H. Zhao, Y. Wang and R. Wang, *Chem. Commun.*, 2014, **50**, 10871–10874.
- 55 C. Zhao, H. Wang, N. Yan, C. Xiao, X. Mu, P. J. Dyson and Y. Kou, *J. Catal.*, 2007, **250**, 33–40.
- 56 K. T. Prabhu Charan, N. Pothanagandhi, K. Vijayakrishna, A. Sivaramakrishna, D. Mecerreyes and B. Sreedhar, *Eur. Polym. J.*, 2014, **60**, 114–122.
- 57 A. Chen, G. Zhao, J. Chen, L. Chen and Y. Yu, *RSC Adv.*, 2013, **3**, 4171–4175.
- 58 A. Dani, V. Crocellà, L. Maddalena, C. Barolo, S. Bordiga and E. Groppo, *J. Phys. Chem. C*, 2016, **120**, 1683–1692.
- 59 N. M. Simon, G. Abarca, J. D. Scholten, J. B. Domingos, D. Mecerreyes and J. Dupont, *Appl. Catal. Gen.*, 2018, **562**, 79–86.
- 60 P. Coupillaud, J. Pinaud, N. Guidolin, J. Vignolle, M. Fèvre, E. Veaudecenne, D. Mecerreyes and D. Taton, *J. Polym. Sci. Part Polym. Chem.*, 2013, **51**, 4530–4540.
- 61 P. Coupillaud, J. Vignolle, D. Mecerreyes and D. Taton, *Polymer*, 2014, **55**, 3404–3414.
- 62 R. Lambert, P. Coupillaud, A.-L. Wirotius, J. Vignolle and D. Taton, *Macromol. Rapid Commun.*, 2016, **37**, 1143–1149.
- 63 R. Marcilla, J. Alberto Blazquez, J. Rodriguez, J. A. Pomposo and D. Mecerreyes, *J. Polym. Sci. Part Polym. Chem.*, 2004, **42**, 208–212.
- 64 K. Vijayakrishna, D. Mecerreyes, Y. Gnanou and D. Taton, *Macromolecules*, 2009, **42**, 5167–5174.
- 65 D. Zhao, Z. Fei, W. H. Ang and P. J. Dyson, *Small*, 2006, **2**, 879–883.
- 66 Q. Meng, M. Hou, H. Liu, J. Song and B. Han, *Nat. Commun.*, 2017, **8**, 14190.
- 67 Y. Liu, Y. Xiang, Y. Zhen and R. Guo, *Langmuir*, 2017, **33**, 6372–6381.
- 68 A. Bouleghimat, M. A. Othman, L. V. Lagrave, S. Matsuzawa, Y. Nakamura, S. Fujii and N. J. Buurma, *Catalysts*, 2017, **7**, 280.
- 69 A. Roucoux, J. Schulz and H. Patin, *Adv. Synth. Catal.*, 2003, **345**, 222–229.
- 70 F. Schwab, M. Lucas and P. Claus, *Green Chem.*, 2013, **15**, 646–649.
- 71 F. Fiévet, S. Ammar-Merah, R. Brayner, F. Chau, M. Giraud, F. Mammeri, J. Peron, J.-Y. Piquemal, L. Sicard and G. Viau, *Chem. Soc. Rev.*, 2018, **47**, 5187–5233.
- 72 M. R. Axet and K. Philippot, *Chem. Rev.*, 2020, **120**, 1085–1145.
- 73 J. A. Widegren and R. G. Finke, *J. Mol. Catal. Chem.*, 2003, **198**, 317–341.
- 74 A. Elaiwi, P. B. Hitchcock, K. R. Seddon, N. Srinivasan, Y.-M. Tan, T. Welton and J. A. Zora, *J. Chem. Soc. Dalton Trans.*, 1995, 3467–3472.
- 75 H. S. Schrekker, M. A. Gelesky, M. P. Stracke, C. M. L. Schrekker, G. Machado, S. R. Teixeira, J. C. Rubim and J. Dupont, *J. Colloid Interface Sci.*, 2007, **316**, 189–195.
- 76 A. S. Pensado and A. A. H. Pádua, *Angew. Chem. Int. Ed.*, 2011, **50**, 8683–8687.
- 77 F. Novio, D. Monahan, Y. Coppel, G. Antorrena, P. Lecante, K. Philippot and B. Chaudret, *Chem. – Eur. J.*, 2014, **20**, 1287–1297.
- 78 E. Bonnefille, F. Novio, T. Gutmann, R. Poteau, P. Lecante, J.-C. Jumas, K. Philippot and B. Chaudret, *Nanoscale*, 2014, **6**, 9806–9816.

Supplementary Information

Tuning the activity and selectivity of polymerised ionic liquid-stabilised ruthenium nanoparticles through anion exchange reactions

Dambarudhar Parida,^{1,2} Camille Bakkali-Hassani,¹ Eric Lebraud,³ Christophe Schatz,¹ Stéphane Grelier,¹ Daniel Taton,¹ Joan Vignolle^{1*}

¹Laboratoire de Chimie des Polymères Organiques (LCPO), University of Bordeaux, F-33607 Pessac Cedex, France

²Swiss Federal Laboratories for Materials Science and Technology (Empa), CH-9014, St. Gallen, Switzerland

³University of Bordeaux, ICMCB, UPR 9048, F-33600 Pessac, France

Corresponding Author

Joan Vignolle

E-mail: joan.vignolle@enscbp.fr

Table of Contents

1. Materials	3
2. General procedures	3
3. Ru content determination by TGA	7
4. TEM Analysis of Ru nanoparticles	9
5. X-ray diffraction (XRD) patterns of Ru NPs	11
6. ζ-potentials of Ru NPs	13
7. XPS analysis	14
8. Catalytic activity	24
9. Activity switching of Ru NPs	26
10. References	27

1. Materials

1-Vinyl-3-imidazolium, 1-chlorobutane, 1-bromobutane, 1-iodobutane, and Poly(vinylpyrrolidone) (MW 55000 g/mol) (PVP) were purchased from Sigma Aldrich, France. Ruthenium chloride hydrate (99.9%) and ruthenium bromide hydrate (99.9%) were purchased from Strem Chemicals. Lithium bis(trifluoromethanesulfonimide) (LiNTf₂) was purchased from TCI France. Ru on Carbon (Ru/C 5%) was purchased from Alfa Aesar France and used as received. HPLC grade solvents were used for synthesis, purification and analysis. All reagents and solvents were used without further purification unless otherwise mentioned.

2. General procedures

(a) *Synthesis of Ionic liquids (monomers) and Polyionic liquids*

1-butyl-3-vinylimidazolium halides (Cl, Br and I) were synthesized following methods reported in the literature.^{1,2} NMR data match those reported in the literature.¹⁻³ Polymerizations of ionic liquids (ILs) were carried out in isopropanol at 70 °C for 24 hours using azobis(2-methylpropionitrile) (AIBN) as thermal initiator. In all cases molar ratio between IL and AIBN was 200 and polymerization was carried out under an inert atmosphere. ¹H NMR analysis after polymerization confirmed 100% conversion of IL(Cl) and IL(Br). Conversion of 75% was obtained in the case of IL(I) after 48 hours of polymerization. Poly(1-butyl-3-vinylimidazolium chloride) (PIL(Cl)) and Poly(1-butyl-3-vinylimidazolium bromide) (PIL(Br)) were precipitated repeatedly in diethyl ether and dried under vacuum (35 °C) till a constant weight was obtained (quantitative yields). PIL(I) was precipitated once in diethyl ether and then taken for dialysis in methanol to remove the remaining IL(I) monomer. After 48 hours of dialysis, PIL(I) was collected by precipitation in diethyl ether and dried under vacuum (35 °C) till a constant weight was obtained with a yield of 60%. Finally, PILs were analyzed by ¹H NMR to confirm the absence of any unreacted monomers, and ¹H NMR spectra of PIL(Cl), PIL(Br), and PIL(I) are given in Figure S1.

Molecular weight and polydispersity index of PILs were determined by the procedure reported by Matyjaszewski et. al.⁴ A GPC system equipped with PSS SDV Linear S (5 µm) column was used at eluent flow-rate of 1 ml/minute. THF containing 10 mmol/L of LiNTf₂ was used as eluent. A viscometer, a multi-angle light scattering detector, and a RI detector from Wyatt Technology were used to acquire elution traces. ASTRA 6.1 software was used for the processing of elution traces. Macromolecular characteristics of different PILs are given in Table S1. For GPC sample preparation anion exchange was carried out on all synthesized PILs to achieve bis(trifluoromethyl)sulfonimide (NTf₂) anion. Typically, 4 molar equivalent LiNTf₂ dissolved in water (10 ml) was added to a 20 ml aqueous solution of PIL(X) (X is Cl or Br) (10 mg/ml) under stirring. The mixture was stirred for 24 hours to ensure a complete exchange of halide anions (Cl⁻ or Br⁻) by NTf₂⁻. Then the precipitate was washed several times with distilled water to remove LiBr and excess LiNTf₂. The product was then dissolved in acetone, precipitated in water, and centrifuged. PIL(NTf₂) obtained was dried under vacuum (35 °C) till a constant weight was obtained (quantitative yield). For anion exchange on PIL(I), AgNTf₂ was used instead of LiNTf₂. In this case, 2 molar equivalent AgNTf₂ dissolved in methanol (10 ml) was added to 20 ml methanol solution of PIL(I) (10 mg/ml) under stirring. After 24 hours, the mixture was centrifuged at 8000 rpm for 15 minutes to remove insoluble AgI. Then, the solution was concentrated by evaporation of methanol and the polymer was recovered by precipitation in water. To ensure complete removal of AgNTf₂, PIL was precipitated twice in water. Finally, it was dried under vacuum (35 °C) till a constant weight was obtained.

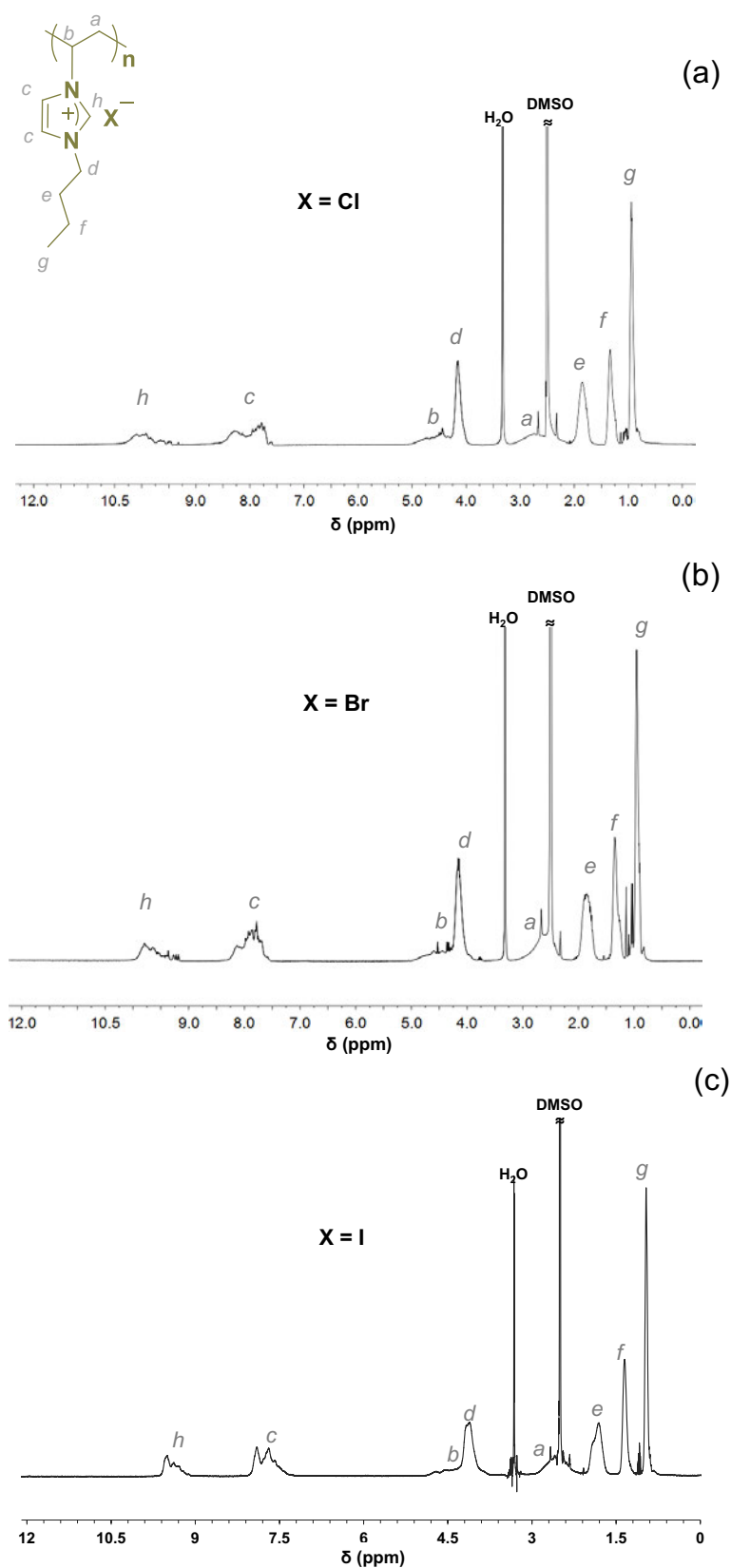
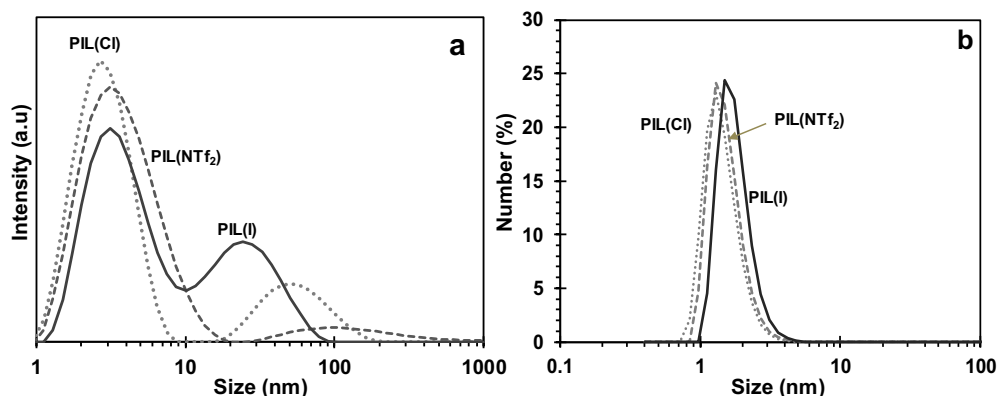


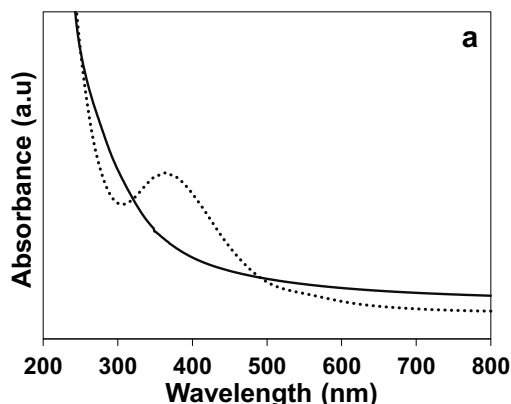
Figure S1. ^1H NMR spectra of (a) Poly(1-vinyl-3-butylimidazolium chloride) (PIL(Cl)) and (b) PIL(Br) and (c) PIL(I). Traces of isopropanol (from the synthesis) appearing at 1.04 ppm are visible.

Table S1. Molecular weight (Mw and Mn) and polydispersity index (PDI) of synthesized PILs.

Entries	Sample	Mw (g/mol)	Mn (g/mol)	PDI
1	PIL(Cl)	59760	33200	1.8
2	PIL(Br)	72576	34560	2.1
3	PIL(I)	59280	45600	1.3
4	PVP	55000 (Sigma)	-	-

**Figure S2.** DLS size of PIL(Cl), PIL(NTf₂) and PIL(I) shown in (a) intensity-average and (b) number average. DLS experiment was carried out at 25 °C using methanol as the common solvent for PILs.**(b) Preparation of Ru nanoparticles**

RuCl₃·xH₂O and RuBr₃·xH₂O were used as metal precursors and PIL(Cl), PIL(Br) or PIL(I) as stabilizers for the synthesis of PIL(X)-stabilized Ru nanoparticles (NPs) (X = Cl, Br, I). The different molar ratio between PIL(X) (IL(X) units) to metal salt (i.e. 50:1, 10:1, 2:1) were used to synthesize PIL(X)@Ru NPs, namely **1-3Cl**, **2Br** and **2I** via polyol process.^{5,6} Typically, 400 mg of PIL(X) and the required quantity of metal salt were dissolved in 40 ml ethylene glycol in a 200 ml schlenk flask. After stirring for 4 hours at 750 rpm, the resulting dark yellow solution was degassed with argon and immersed in an oil bath preheated at 170 °C. The dark yellow solution slowly turned black, indicating the formation of Ru(0)NPs. Heating was continued for 1.5 hours to ensure complete conversion of ruthenium salt to Ru(0) and formation of NPs which was confirmed by UV-vis spectroscopy analysis. The disappearance of the broad absorption band in the spectrum of the precursor after reduction indicates complete reduction of Ru(+2) into Ru(0). A representative example is given in Figure S3 with the reduction of RuCl₃ in presence of PIL(Cl). PILs stabilized NPs were collected by centrifuging 5 ml of NP solution with 30 ml of a mixture of diethyl ether and acetone (50:50). After this initial centrifugation, RuNPs were dissolved in acetone (15 ml) and diethyl ether was added (20 ml); the resulting suspension was then subjected to centrifugation. This step was repeated one more time. The resulting sticky black product was next dissolved in 5 ml of methanol and centrifuged with 25 ml of diethyl ether. All centrifugations were carried out at 8000 rpm for 15 min at 15 °C. The resulting shiny black product was vacuum (0.8 mmHg) dried at 35 °C till a constant weight was obtained (24 - 48h). This step ensures the removing of the different solvents, including ethylene glycol (b.p. = 197°C). The same procedure was followed for the preparation of PVP-stabilized RuNPs and 1-Butyl-3-methylimidazolium bromide-stabilized RuNPs.



SUPPORTING INFORMATION

Figure S3. UV-Vis spectra of precursor solution ($\text{RuCl}_3 + \text{PIL}(\text{Cl})$) showing the characteristic absorption band (dotted line) of RuCl_3 around 365 nm and diffused absorption band was observed after reduction (solid line). Diffused absorption indicates the complete reduction of RuCl_3 and formation of very small Ru nanoparticles.^{7,8}

(c) Anion exchange on PILs stabilized Ru NPs

Anion exchange via LiNTf_2 : To change the solubility and study the effect of anion on the catalytic activity of Ru NPs, anion exchange was carried out on **2Br**. In a typical anion exchange reaction, 10 ml aqueous solution of LiNTf_2 (4 molar equivalent) was added dropwise to 30 ml aqueous solution (1.5 mg/ml) of **2Br** under vigorous stirring, leading to the slow precipitation of **2NTf₂**. To ensure complete anion exchange, the mixture was stirred for 16 hours under ambient temperature (see also XPS data in Figures S14 and S15). All operations were carried out under an argon atmosphere. The resulting precipitates were washed several times with water and then dried under vacuum at 35 °C till a constant weight was obtained. After anion exchange, NPs became hydrophobic and soluble in organic solvents, as given in the solubility chart (Table S1). The same procedure was used for the preparation of **2NTf₂** and **2PF₆** from **2Br**. For the preparation of **2PF₆**, LiPF_6 was used as the salt.

Anion exchange via AgNTf_2 : **2I** being not soluble in water, a mixture of methanol (MeOH) and water (70-30) was used to obtain a stable solution of **2I**. The addition of a LiNTf_2 solution (MeOH + H_2O) to the solution of **2I** (following a similar procedure to that described for **2Cl** and **2Br**) led to quick precipitation of the product. In this case, XPS analysis revealed that only 20% of iodide was replaced by NTf_2 . Therefore, the anion exchange procedure was modified to achieve complete exchange. In a typical procedure, 30 mg of **2I** was dissolved in 15 ml of methanol. 200 mg AgNTf_2 pre-dissolved in 15 ml of methanol was slowly added to the solution and stirred overnight. All the operation was carried out under an argon atmosphere. The mixture was centrifuged at 8000 rpm for 15 minutes to separate AgI (light yellow precipitate). The clear black solution obtained was reduced to ~5 ml by evaporation. Excess of AgNTf_2 was removed by dialysis of the solution in distilled water. After 24 hours, the resulting black precipitate was collected and washed several times with distilled water. It is worth mentioning here that, during dialysis, $\text{Ru}(0)$ may get converted to its oxide and can adversely affect the catalytic activity of NPs. To reduce the amount of Ru oxide in the final sample, dialyzed NPs were subjected to an additional reduction step. In this step, a 5 ml solution of dialyzed NP (in methanol) was stirred for 16 hrs at 50 °C under 5 bars of hydrogen pressure. Then it was dried under vacuum at 35 °C till a constant weight was obtained.

2Br^I was obtained by anion exchange between **2NTf₂** and an excess of LiBr . In this case, **2NTf₂** was dissolved in acetone (1.5 mg/ml) and LiBr (4 molar equivalent) pre-dissolved in acetone was added dropwise under stirring. The mixture was stirred for 16 hours to ensure a complete exchange of NTf_2^- with Br^- . Upon anion exchange, **2Br^I** precipitated out of the solution, after being washed with acetone and centrifuged twice to remove excess LiBr , **2Br^I** was dried under vacuum at 35 °C till a constant weight was obtained.

Anions Solvents	2Cl	2Br	2I	2NTf ₂	2Br ^I	PVP
H ₂ O	✓	✓			✓	✓
Methanol	✓	✓	✓	✓	✓	✓
C ₃ H ₈ O	✓	✓	✓		✓	
CHCl ₃	✓	✓	✓		✓	✓
CH ₂ Cl ₂	✓	✓	✓		✓	✓
THF				✓		
C ₄ H ₈ O ₂				✓*		

(✓) indicates solubility of catalyst in the respective solvent.

***2NTf₂** is partially soluble in ethyl acetate.

†**2PF₆** is not soluble at room temperature but forms a sticky substance at high temperature (around 100 °C)

3. Ru content determination by TGA

Ru content of all NP samples was determined by thermogravimetric analysis (TGA) using a TGA Q-500 from TA instruments. A typical TGA curve of **PIL(Cl)** (a), **2Cl** (b), and **2Br** (c) are shown in Figure S4. Initially, samples were heated in a nitrogen environment till 600 °C and subsequently in the air till 750 °C. Residual weight obtained after the introduction of air was considered as the Ru content.

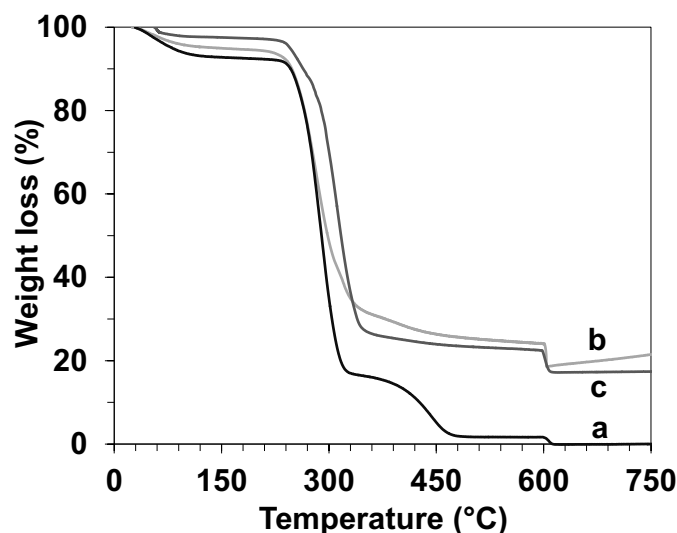


Figure S4. TGA curve of (a) **PIL(Cl)** (b) **2Cl** and (c) **2Br** showing weight loss with temperature. Residual weight after 600 °C was considered as the Ru content of the samples.

Table S3. Ru content of NP samples determined by TGA.

Entries	Sample	Ru content (%)
1	1Cl	9.8
2	2Cl	18.1
3	3Cl	29
4	2Br	17.1
5	2I	11.2
6*	IL(Cl)@RuNP	13.9
7 [#]	PVP@RuNP	10.1
8	2NTf ₂	9.3
9 [†]	2NTf ₂	5.7
10	2Br [†]	17.6

*Ru NPs obtained by using 1-Butyl-3-ethylimidazolium bromide (IL).

[#]PVP stabilized Ru NPs.

[†]Obtained from 2I via anion exchange with AgNTf₂.

4. TEM analysis of Ru nanoparticles

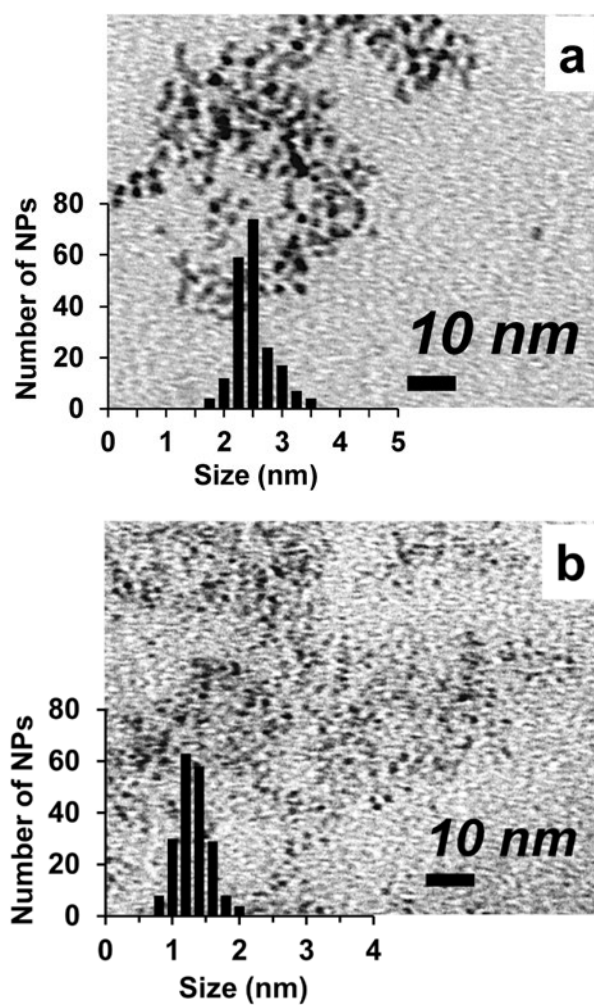


Figure S5. TEM images of (a) **2Br** and (b) **2I**.

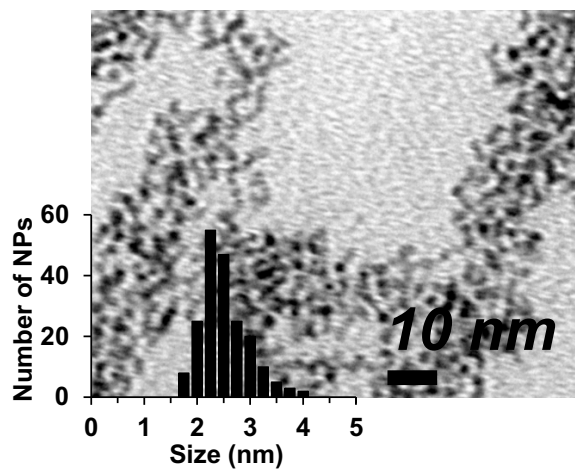


Figure S6. (a) TEM images of **2NTf₂** resulting from the anion exchange between **2Br** and LiNTf₂. No change in the size of the particles was observed after anion exchange.

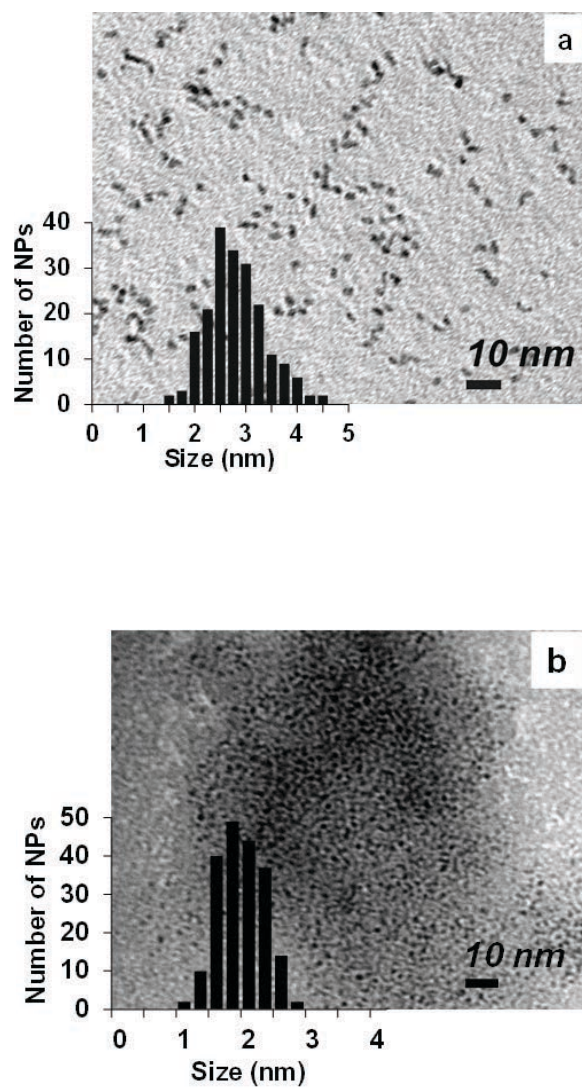


Figure S7. TEM images of Ru NPs synthesized using (a) Poly(vinylpyrrolidone) (PVP@RuNP) and (b) 1-Butyl-3-ethylimidazolium bromide (IL@RuNP). Note: 0.1 molar equivalents of $\text{RuCl}_3 \cdot \text{XH}_2\text{O}$ was used with respect to monomeric unit.

5. X-ray diffraction (XRD) patterns of Ru NPs

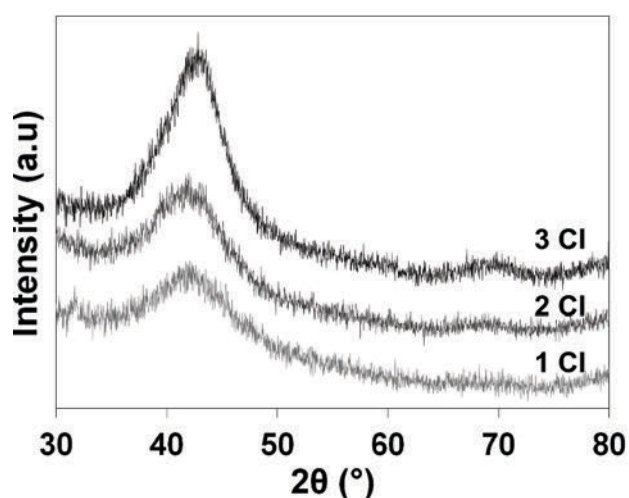


Figure S8. Powder XRD pattern of Ru NPs synthesized using PIL(Cl). The peak corresponding to Ru (101) plane can be seen at 43° (2θ).^{9,10} With an increase in precursor (RuCl_3) loading from 1Cl to 3Cl, the sharpening of the peak for the 101 plane is in agreement with an increase in NP size.

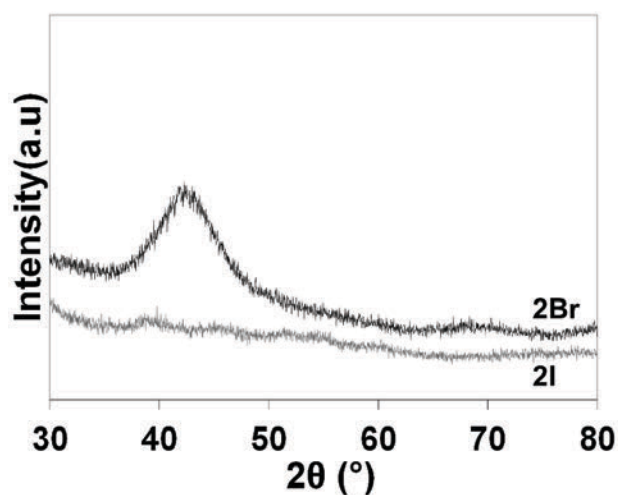


Figure S9. Powder XRD pattern of 2Br and 2I. In the case of 2I (1.2 nm by TEM, Figure S3), the sizes of the crystalline domains are too small to observe a signal.¹¹

Table S4. Size of different Ru NPs determined by TEM and XRD analysis.

Sample	NP size (nm) by TEM	NP size (nm) by XRD (Debye-Scherrer relation)
1Cl	1.47 ± 0.25	1.10
2Cl	2.55 ± 0.38	1.26
3Cl	2.65 ± 0.75	1.39
2Br	2.30 ± 0.30	1.33
2I	1.21 ± 0.24	-
IL(Cl)@RuNP*	1.8 ± 0.33	-
PVP@RuNP	2.70 ± 0.56	-
2NTf ₂	2.40 ± 0.45	-
2Br ^l	2.35 ± 0.55	2.0

*Nano particles synthesized using 1-Butyl-3-ethylimidazolium bromide.

6. ζ -potentials of Ru NPs

ζ -potentials of all NPs were measured at 25 °C by Malvern Zetasizer ZS. ζ -potentials were measured in water for **1-3Cl**, **2Br**, and PVP@RuNP (Table S5) and in MeOH for **1-3Cl**, **2Br**, **2I**, **2NTf₂** and PVP@RuNPs (Table S6).

Table S5. ζ -potential of PILs and PVP stabilized Ru NPs in water.

Sample	ζ -potentials in water (mV)
1Cl	55.5 ± 2.4
2Cl	49.4 ± 0.5
3Cl	34.9 ± 1.6
2Br	58.3 ± 1.1
PVP@RuNP	8.2 ± 0.4

Note: ζ -potential was measured at 25 °C.

Table S6. ζ -potentials of PILs and PVP stabilized Ru NPs in methanol.

Sample	ζ -potential (mV)
1Cl	38.0 ± 1.4
2Cl	38.0 ± 0.8
3Cl	37.2 ± 1.3
2Br	40.0 ± 1.1
2NTf ₂	41.8 ± 1.1
2I	40.1 ± 1.1
PVP@RuNP	2.6 ± 0.3

Note: ζ -potential was measured at 25 °C.

7. XPS analysis

X-ray photoelectron spectroscopy (XPS) analysis was carried out on PIL(X) and PIL(X)@RuNPs to study the nature of the interaction between PILs and RuNPs. K-Alpha X-ray Photoelectron Spectrometer from Thermo Fisher Scientific equipped with monochromatized AlK α source ($h\nu=1486.6$ eV) was used for surface analysis. The full spectra (0-1350eV) and high-resolution spectra were recorded with a constant pass energy of 200 eV and 40 eV respectively. Ar⁺ sputtering was used for depth profiles. High-resolution spectra were processed and fitted with AVANTAGE software from Thermo Fisher Scientific. All the scans were corrected considering C(1s) as the reference (285.0 eV).^{12,13}

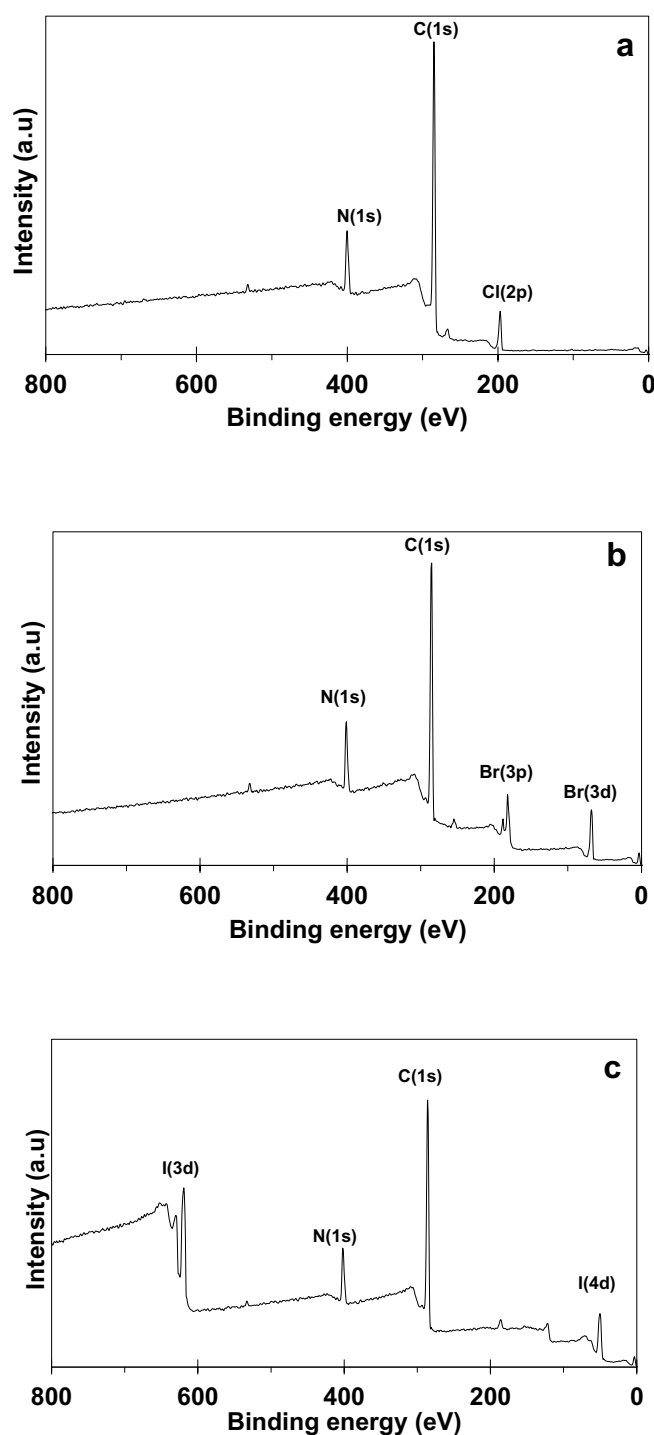


Figure S10. XPS survey scan of (a) PIL(Cl), (b) PIL(Br) and (c) PIL(I).

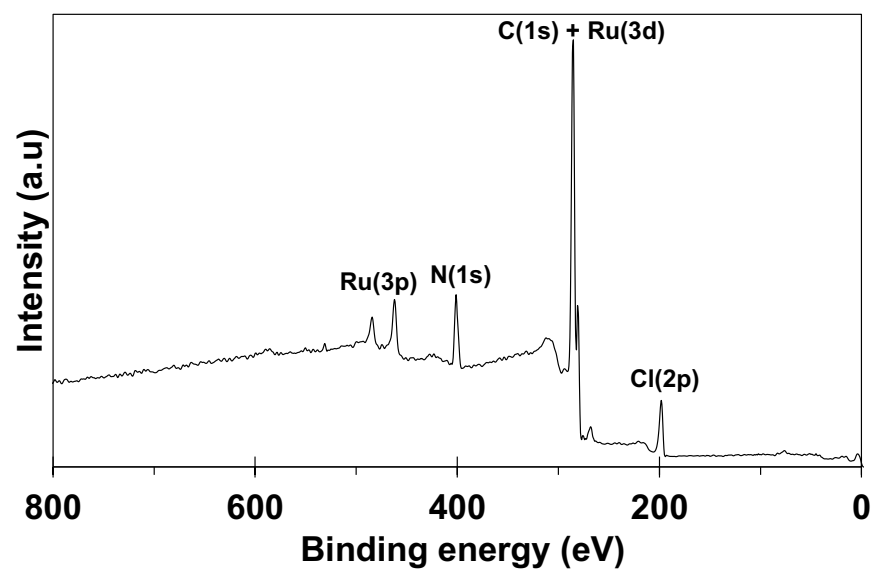


Figure S11. XPS survey scan of PIL(Cl) stabilized Ru NP (2Cl).

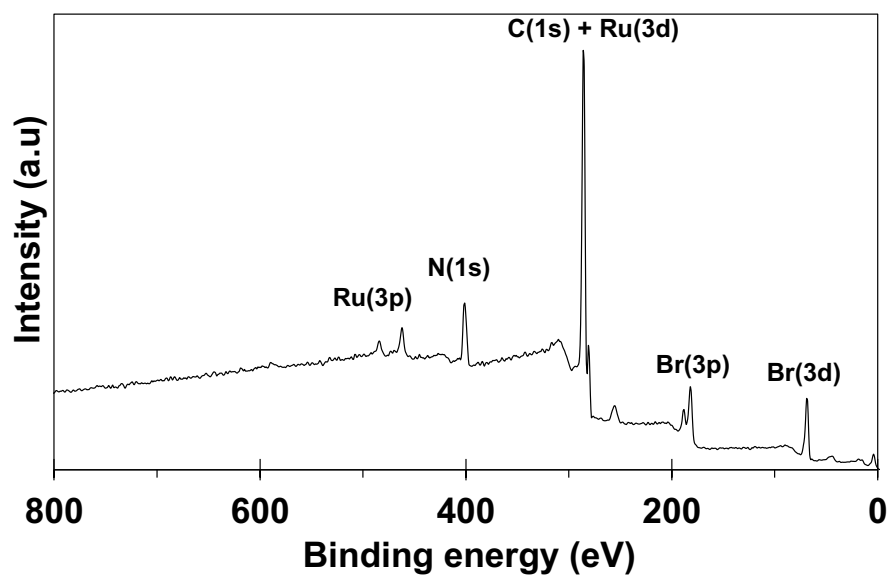


Figure S12. XPS survey scan of PIL(Br) stabilized Ru NP (2Br).

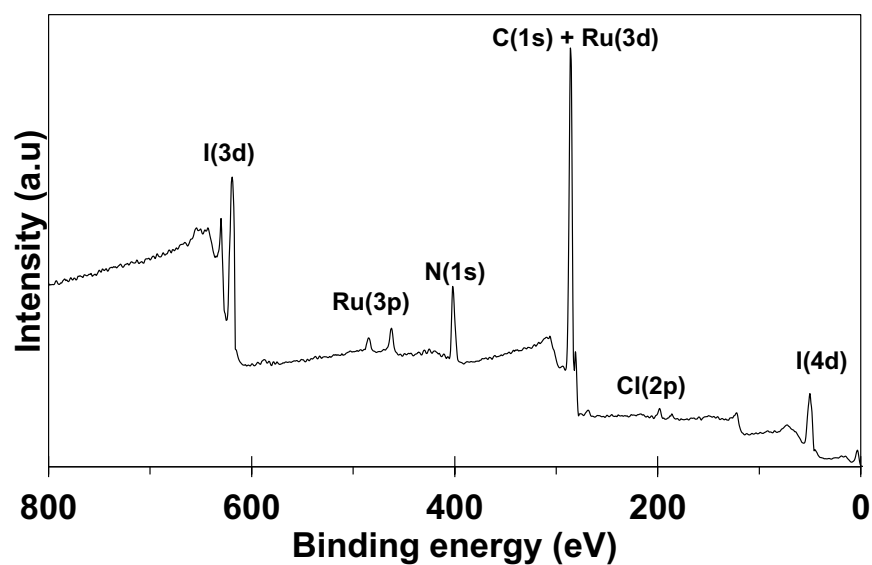


Figure S13. XPS survey scan of **2I**. The presence of Cl(2p) peak can be attributed to the exchange of I^- by Cl^- (2%) during NP synthesis using RuCl_3 as a precursor.

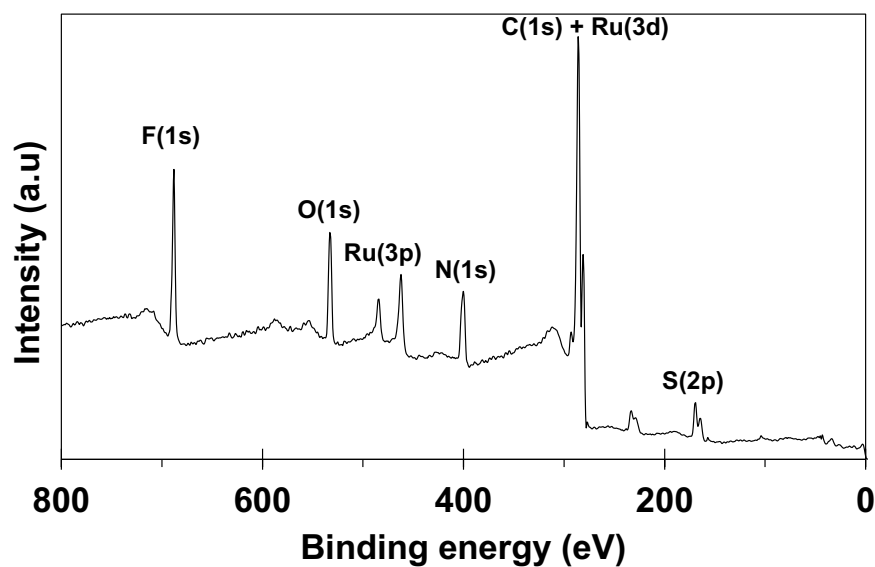


Figure S14. XPS survey scan of **2NTf₂** NPs obtained after anion exchange between **2Br** and LiNTf_2 . The absence of any characteristic peak for Br is a sign of the complete exchange of Br^- by NTf_2^- .

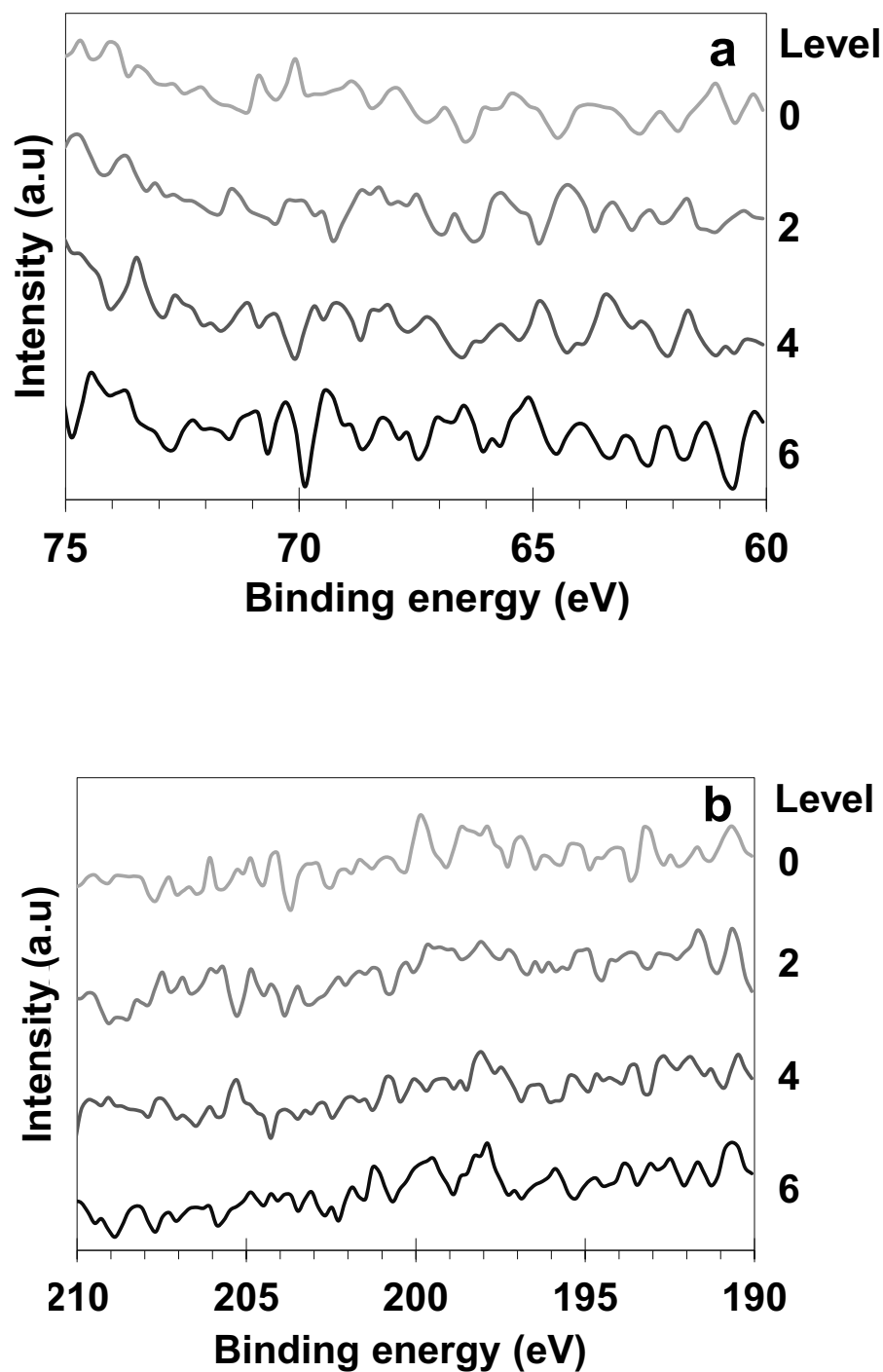


Figure S15. High-resolution XPS scan of (a) Br(3d) region of 2NTf_2 at different depths. The absence of Br(3d) peak indicates the complete replacement of Br^- by NTf_2^- . (b) Cl 2P region scan of 2NTf_2 (prepared from 2Cl) at different depths. The absence of Cl 2p peak indicates complete replacement of Cl^- by NTf_2^- during anion exchange

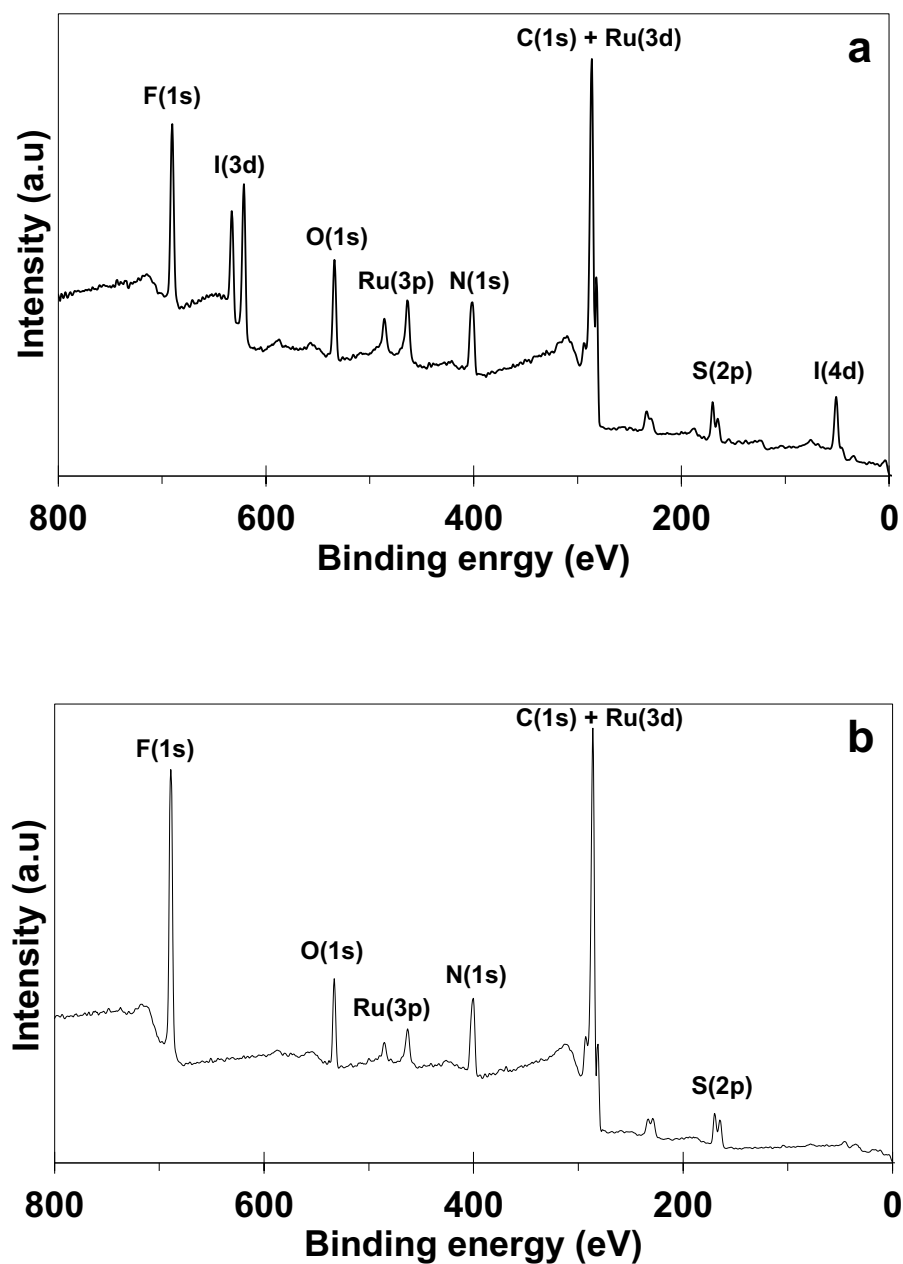


Figure S16. (a) XPS survey scan of NPs obtained after anion exchange between **2I** and LiNTf₂. A strong peak of I(3d) at 614 eV indicates the partial replacement of I⁻ by NTf₂⁻ (~21%). (b) XPS survey scan of NPs obtained after anion exchange between **2I** via AgNTf₂, absence of characteristic peak of iodide indicates successful exchange of I⁻ by NTf₂⁻.

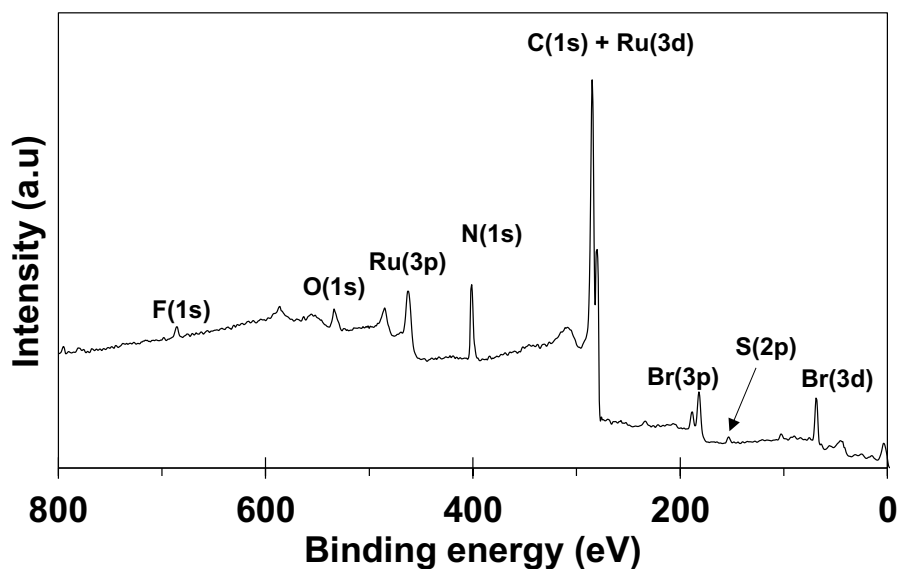


Figure S17. XPS survey scan of **2BrI** resulting from the anion exchange reaction between **2NTf₂** and LiBr. F(1s) and S(2p) peaks in the scan is due to some residual (~8 %) NTf₂⁻ in the sample.

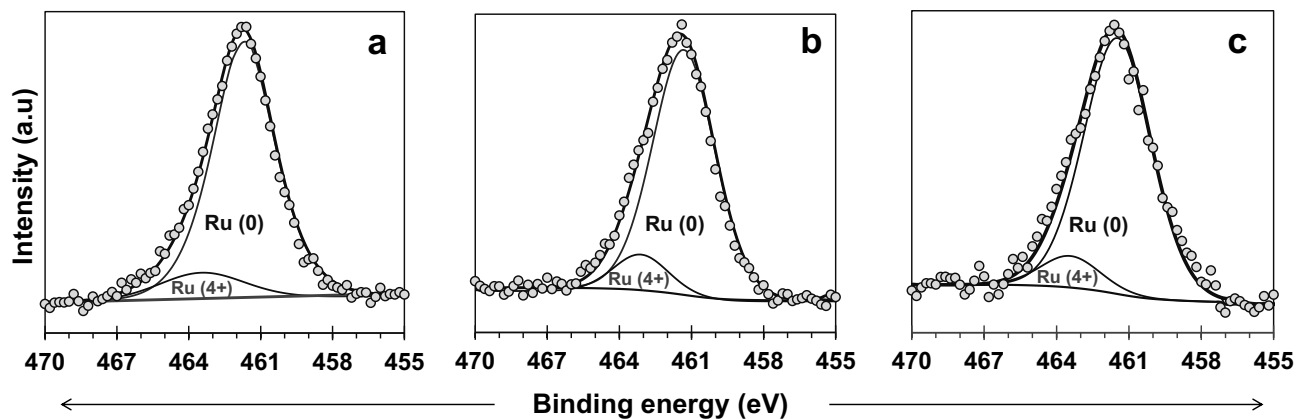


Figure S18. High resolution Ru(3p) scan of (a) **2ClI**, (b) **2BrI** and (c) **2II**. Deconvolution of Ru(3p) shows different oxidation states of Ru present in PILs stabilized NPs. From the figures, it is evident that NPs are mainly composed of Ru(0) (at 461.4 eV) and a small proportion of Ru(4+) towards higher BE (463.4 eV).¹⁴⁻¹⁶

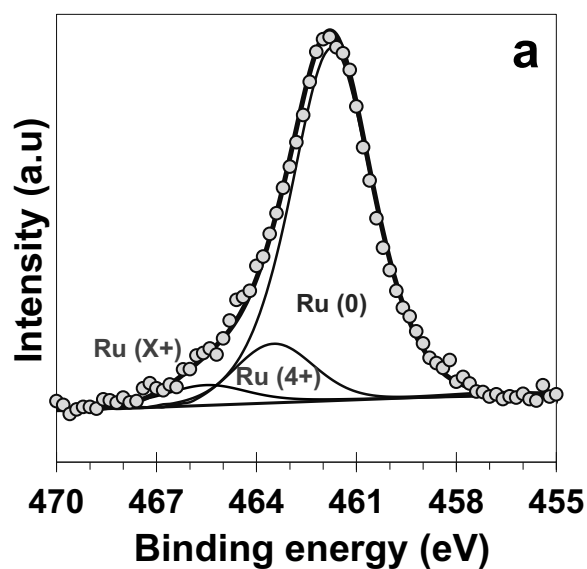


Figure S19. High-resolution Ru(3p) scan showing different oxidation states of Ru present in 2NTf₂. An additional high binding energy component assigned to Ru(X+) (at 465.9 eV) was detected,^{15,17} which results from the exposure to air during purification after anion exchange.

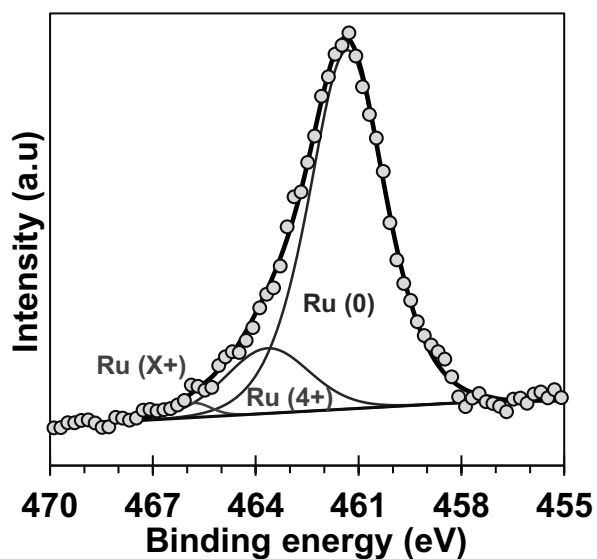
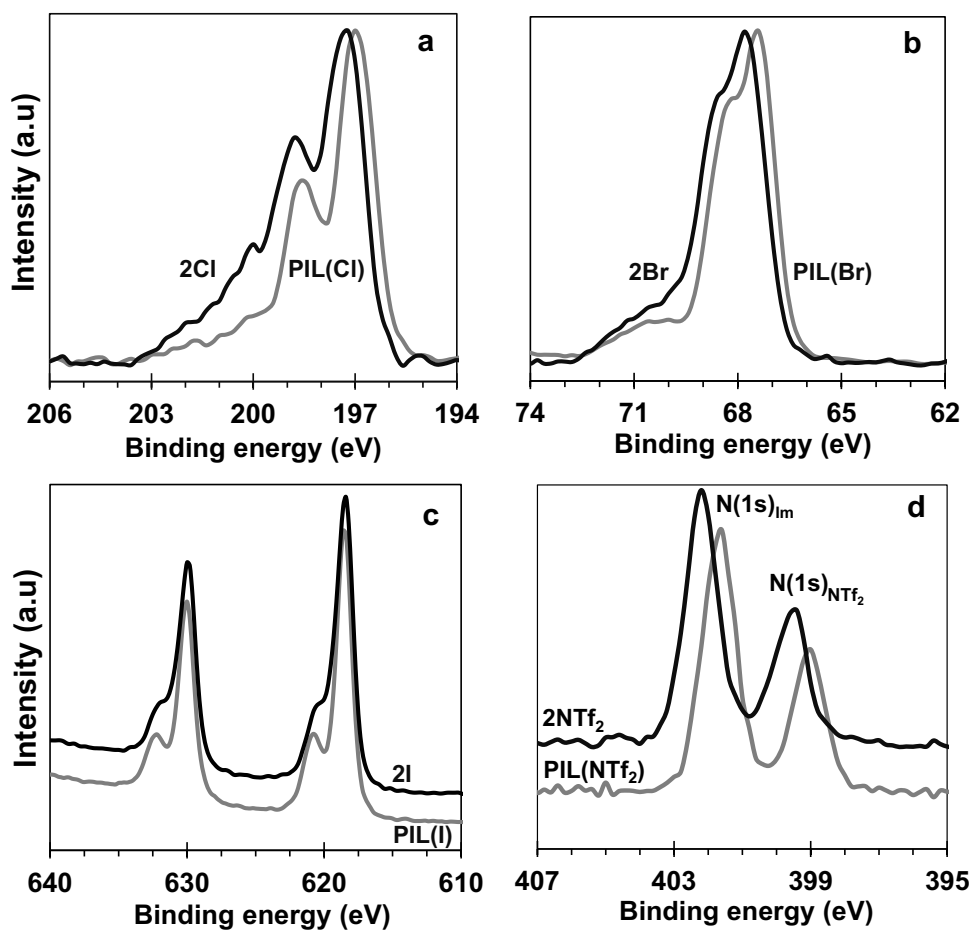


Figure S20. High-resolution scan of Ru(3p) showing different oxidation states of Ru present in 2BrI.

Table S7. Different oxidation states of Ru and their proportion in NPs determined by deconvolution of Ru(3p) scan.

Entry	Sample	Position of peaks and Ru(0) composition		
		Ru(0) [Area %]	Ru(4+) [Area %]	Ru(X+) [Area %]
1	2Cl	461.3 [88.4]	463.4 [11.6]	-
2	2Br	461.4 [91.5]	463.4 [8.5]	-
3	2NTf ₂	461.4 [85.1]	463.4 [10.3]	465.9 [4.6]
4	2Br ^I	461.4 [82.7]	463.4 [15.7]	465.9 [1.6]
5	2I	461.4 [90.3]	463.4 [9.7]	-

**Figure S21.** Overlay of high resolution XPS scan of (a) Cl(2p) region of PIL(Cl) and 2Cl, (b) Br(3d) region of PIL(Br) and 2Br, (c) I(3d) region of PIL(I) and 2I and of (d) N(1s)_{Im} and N(1s)_{NTf₂} in PIL(NTf₂) and 2NTf₂.

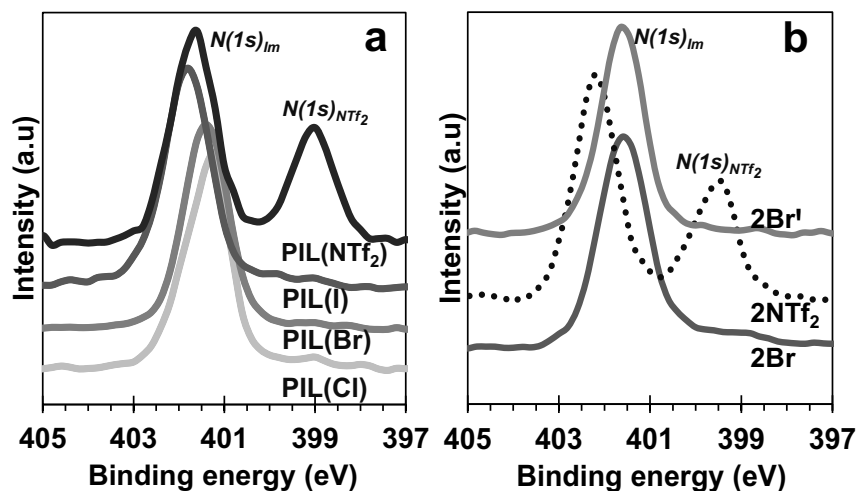


Figure S22. High-resolution XPS scan in N(1s) region of (a) PILs showing the shift in the binding of imidazolium N(1s) in presence of different anions (b) showing the change in the BE of N(1s)Im before anion exchange (**2Br**), after Br/NTf₂ anion exchange (**2NTf₂**) and after NTf₂/Br anion exchange (**2Br'**). The same BE observed for N(1s)Im in both **2Br** and **2Br'** suggest that a similar environment around the surface of Ru NPs (to that of the starting **2Br**) has been recovered after two successive anion exchange reactions.

The signals corresponding to the binding energy (BE) of all halogen atoms (Cl, Br, I) appear as (non-symmetrical) doublets because of spin-orbit couplings. The value of the BE of the anion was given according to the most intense component of the doublet that appears at the lowest BE (Table S8). All halogens feature both in the “free” PIL(X) (X= Cl, Br, I) and in the corresponding PIL(X)@RuNPs (**2Cl**, **2Br**, **2I**) a minor signal that appears at relatively higher BE compared to the most intense signals. Although it is difficult to attribute a specific environment to each signal, we may hypothesize that the difference in BE between the major and minor signals could be related to the number or nature of interactions between the different anions and the C₂-H, C₄-H, and C₅-H by H-bonding.¹⁸ The major signal appearing at the lowest BE would then correspond to a situation where the anion is involved in a fewer H-bond (1 or 2) compared to the minor signal at higher BE, which would be involved in multiple H-bonds (2 or more). For simplicity, only discussions about the BE of the major signals and their shifts between the polymer and the corresponding NP have been included in the main text. In the case of the NTf₂ anion, binding to the Ru surface could occur either via the N atom or via the O atoms¹⁸ but XPS analysis does not allow to rule out one of those interactions.

In the case of the iodide anion, the absence of a shift in the BE of I(3p) between PIL(I) and the respective NP (**2I**) suggests that I[−] do not interact significantly with the metal surface. In contrast, the shift of the N(1s) of the imidazolium moieties N(1s)Im toward lower BE observed in the XPS spectrum of **2I** (compared to that observed in PIL(I)) suggests an interaction between the imidazolium cation and the Ru surface. We may hypothesize that the imidazolium cation lies parallel to the surface by analogy with the stabilization of gold NPs in imidazolium-based ILs (see Figure S23).²⁰ However, the interaction of the imidazolium cation with the Ru surface via the C₄-H/C₅-H or via the C₂-H might also be postulated (Figure S23).¹⁹ As a result of this cation-surface interaction, the surface becomes seriously hindered, which certainly prevents aromatic moieties to adsorb by “ π -stacking” onto the flat surface. Nevertheless, this interaction does not prevent the binding of alkenes to the edges or corners of **2I**, which allows unsaturated substrates, such as styrene, to undergo selective hydrogenation of the C=C bond.

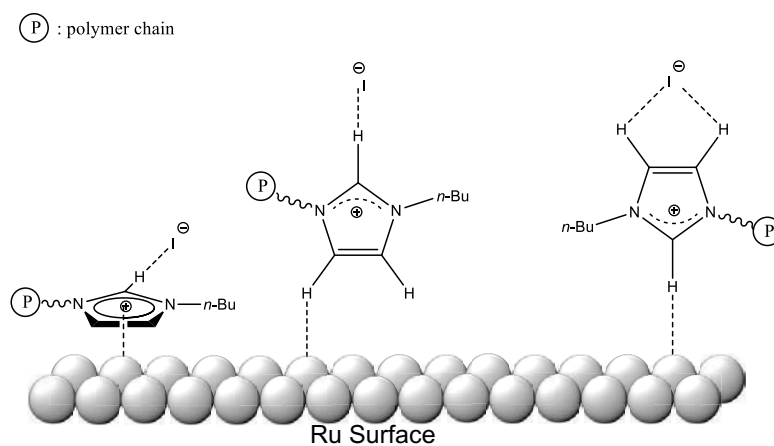


Figure S23. Schematic representations of possible interactions between the imidazolium cation and the RuNP surface in the case of **2I**.

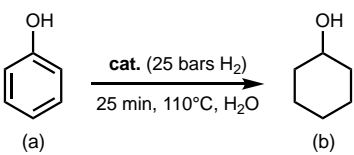
Table S8. The binding energy of different elements in PIL(X) (X = Cl, Br, I, NTf₂) and in the corresponding PIL stabilized Ru NPs.

Sample	C(1s)	N(1s) _{im}	Anion	Ru	
			Cl (2p)	3d	3p
PIL(Cl)	285.0	401.2	197.0	-	-
2Cl	285.0	401.6	197.2	280.2	461.4
			Br (3d)	3d	3p
PIL(Br)	285.0	401.4	67.4	-	-
2Br	285.0	401.6	67.8	280.4	461.4
			I (3d)	3d	3p
PIL(I)	285.0	401.8	618.4	-	-
2I	285.0	401.6	618.4	280.4	461.6
			NTf ₂ (N1s)	3d	3p
PIL(NTf ₂)	285.0	401.6	399.0 (N)	-	-
2NTf ₂	285.0	402.2	399.4 (N)	280.8	461.8

8. Catalytic activity

(a) Hydrogenation of phenol by Ru NPs

Table S9. Hydrogenation of Phenol in water by PILs, ionic liquid and PVP stabilized Ru NPs.



(a) $\xrightarrow[25 \text{ min, } 110^\circ\text{C, H}_2\text{O}]{\text{cat. (25 bars H}_2\text{)}}$ (b)

Entries	Catalyst	Conversion (%)	Selectivity (b %)	Remark
1	2Br	100	100	-
2	2Cl	100	100	The catalyst was recycled (fig. S24)
3	IL(Cl)@RuNPs	100	100	Formation of bulk metal
4	PVP@Ru	100	100	Aggregation of NPs

Hydrogenation were performed at 110 °C for 25 min, using 25 bars of H₂, 0.166 mol.% of Ru and water as solvent. Conversion was determined by determined by ¹H NMR.

(b) Recycling of PIL stabilized Ru NP (2Cl) during hydrogenation of phenol in water

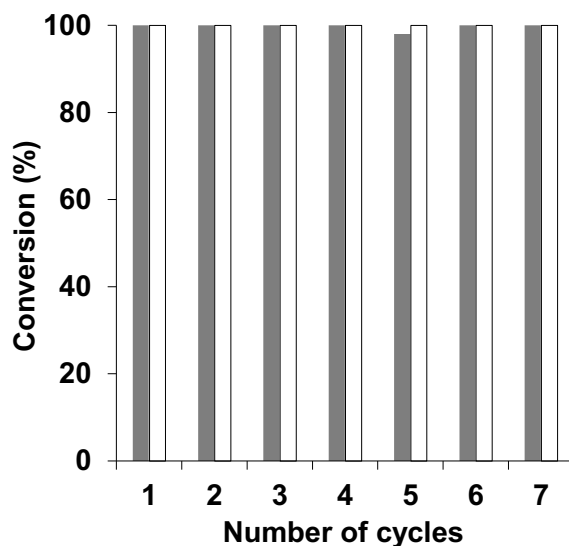


Figure S24. Activity and selectivity of 2Cl during recycling. Phenol was used as a substrate at 0.166 mol% Ru loading, 25 bars of H₂, and 110 °C. Hydrogenation time was kept 25 minutes for every cycle. Grey bars represent phenol conversion and the white bar indicates cyclohexanol selectivity. At every cycle, complete hydrogenation of phenol to cyclohexanol indicates remarkable stability of PIL stabilized Ru nanoparticles.

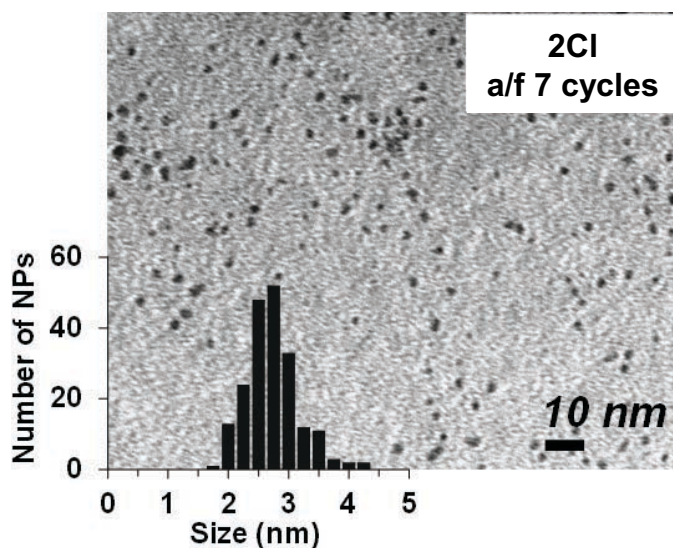


Figure S25. TEM image of 2Cl after 7th hydrogenation cycle. From the particle size and distribution, it can be confirmed that PILs stabilized RuNPs do not agglomerate even after multiple hydrogenation cycles under the hydrogenation conditions (Phenol hydrogenation at 110 °C for 25 min, using 25 bar of H₂ and 0.166 mol.% of Ru).

(c) Catalyst poisoning by CS₂

To confirm the heterogeneous nature of Ru NP catalysts, CS₂ poisoning test was carried out on 2Cl during hydrogenation of phenol in water.^{21, 22} Hydrogenation was started as per the procedure described in section 2d. The reaction temperature was maintained at 30 °C. After the desired time, the reactor was depressurized to collect the sample for determining phenol conversion. At this time, CS₂ dissolved in THF was injected (0.5 molar equivalents relative to Ru) into the reactor followed by re-pressurization with H₂. Then the reactor was immersed in the preheated oil bath (30 °C) to start the hydrogenation. After 4 hours, the reactor was cooled down and depressurized to stop the reaction. The product was extracted with diethyl ether and taken for ¹H NMR analysis upon evaporating diethyl ether (no vacuum). GC-MS analysis was also carried out to confirm conversions (Figure S26).

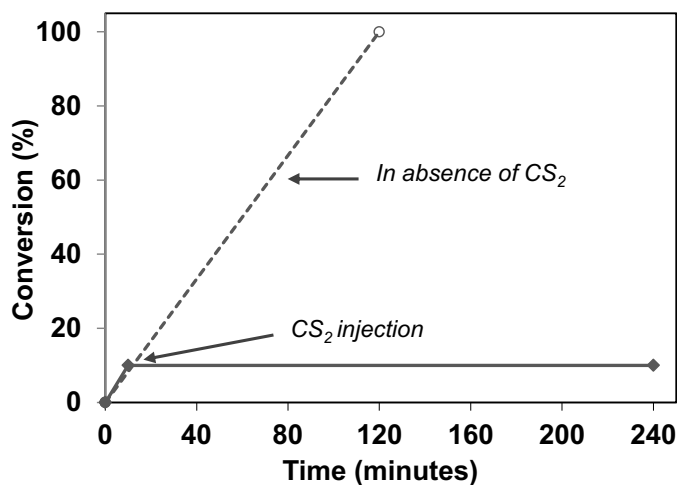


Figure S26. Plot showing phenol conversion in the absence (dotted line) and presence (solid line) of CS₂. After the addition of CS₂ (at 10 min), conversion remained unchanged which is the characteristic of heterogeneous hydrogenation. Hydrogenation was carried out at 0.166 mol% Ru loading, 25 bar H₂, 30 °C.

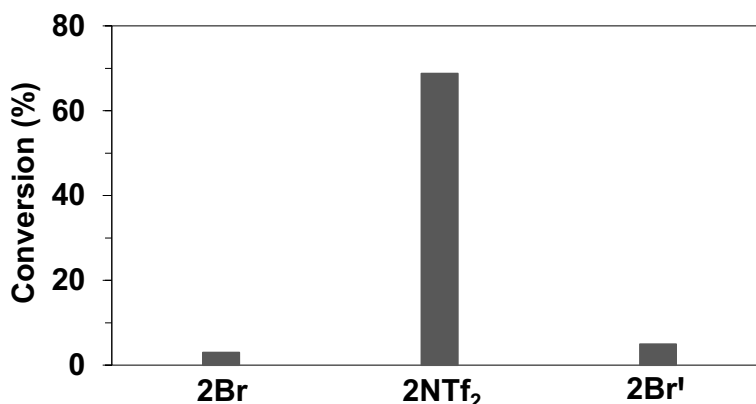
(d) Toluene hydrogenation using 2NTf₂**Table S10.** Influence of solvent on the catalytic activity of 2NTf₂ during hydrogenation of Toluene.

Entries	Ru NP	Solvent	Conversion of toluene (%)
1	2NTf ₂	MeOH	70
2	2NTf ₂	THF	100
3*	2NTf ₂	Ethyl Acetate	65

Hydrogenation was performed at 110 °C for 60 min in the required quantity of solvent, using 25 bars of H₂ and 0.33 mol.% of Ru. In all cases, conversion was determined by GC-MS.

*2NTf₂ is partially soluble in Ethyl acetate.

9. Activity switching of Ru NPs

**Figure S27.** Demonstrating activity switching of PIL(Br) stabilized Ru NPs (2Br) by simple anion exchange route. All hydrogenation experiments were carried out using toluene as a substrate at 0.33% Ru loading, 25 bars H₂, and 100 °C for 60 mins.

10. References

1. R. Marcilla, J. B. Alberto, J. Rodriguez, J. A. Pomposo and D. Mecerreyes, *J. Polym. Sci., Part A: Polym. Chem.*, 2004, **42**, 208-212.
2. Y. Rong, Z. Ku, M. Xu, L. Liu, M. Hu, Y. Yang, J. Chen, A. Mei, T. Liu and H. Han, *RSC Adv.*, 2014, **4**, 9271-9274.
3. R. Thenarukandiyil, H. Thrikkykkal and J. Choudhury, *Organometallics*, 2016, **35**, 3007-3013.
4. H. He, M. Zhong, B. Adzima, D. Luebke, H. Nulwala and K. Matyjaszewski, *J. Am. Chem. Soc.*, 2013, **135**, 4227-4230.
5. M. Ohtaki, M. Komiyama, H. Hirai and N. Toshima, *Macromolecules*, 1991, **24**, 5567-5572.
6. L. S. Sarma, C.-H. Chen, S. M. S. Kumar, G.-R. Wang, S.-C. Yen, D.-G. Liu, H.-S. Sheu, K.-L. Yu, M.-T. Tang, J.-F. Lee, C. Bock, K.-H. Chen, B.-J. Hwang, *Langmuir*, 2007, **23**, 5802-5809.
7. X. Yan, H. Liu and K. Y. Liew, *J. Mater. Chem.*, 2001, **11**, 3387-3391.
8. H. Erdoğan, Ö. Metin and S. Özkar, *Catal. Today*, 2011, **170**, 93-98.
9. M. Fang, N. Machalaba and R. A. Sanchez-Delgado, *Dalton Trans.*, 2011, **40**, 10621-10632.
10. H. Jang, S.-H. Kim, D. Lee, S. E. Shim, S.-H. Baek, B. S. Kim and T. S. Chang, *J. Mol. Catal. A: Chem.*, 2013, **380**, 57-60.
11. S. Mourdikoudis, R. M. Pallares, Nguyen T. K. Thanh, *Nanoscale*, 2018, **10**, 12871-12934.
12. N. Chakroune, G. Viau, S. Ammar, L. Poul, D. Veautier, M. M. Chehimi, C. Mangeney, F. Villain, F. Fiévet, *Langmuir*, 2005, **21**, 6788-6796.
13. T. Cremer, C. Kolbeck, K. R. J. Lovelock, N. Paape, R. Wölfel, P. S. Schulz, P. Wasserscheid, H. Weber, J. Thar, B. Kirchner, F. Maier and H.-P. Steinrück, *Chem. Eur. J.*, 2010, **16**, 9018-9033.

SUPPORTING INFORMATION

14. Yang, J., Lee, J. Y., Deivaraj, T. C., Too, H.-P. Preparation and characterization of positively charged ruthenium nanoparticles. *J. Colloid Interface Sci.* **271**, 308-312.
15. M. Zawadzki and J. Okal, *Mater. Res. Bull.*, 2008, **43**, 3111-3121.
16. J. L. Gómez de la Fuente, M. V. Martínez-Huerta, S. Rojas, P. Hernández-Fernández, P. Terreros, J. L. G. Fierro and M. A. Peña, *Appl. Catal., B: Environmental*, 2009, **88**, 505-514.
17. K. Qadir, S. H. Joo, B. S. Mun, D. R. Butcher, J. R. Renzas, F. Aksoy, Z. Liu, G. A. Somorjai and J. Y. Park, *Nano Lett.*, 2012, **12**, 5761-5768.
18. A. Elaiwi, P. B. Hitchcock, K. R. Seddon, N. Srinivasan, Y.-M. Tan, T. Welton and J. A. Zora, *J. Chem. Soc. Dalton Trans.*, 1995, 3467-3472.
19. A. S. Pensado and A. A. H. Pádua, *Angew. Chem. Int. Ed.*, 2011, **50**, 8683-8687.
20. H. S. Schrekker, M. A. Gelesky, M. P. Stracke, C. M. L. Schrekker, G. Machado, S. R. Teixeira, J. C. Rubim and J. Dupont, *J. Colloid Interface Sci.*, 2007, **316**, 189-195.
21. L. M. Rossi and G. Machado, *J. Mol. Catal. A: Chem.*, 2009, **298**, 69-73.
22. C. Vollmer, E. Redel, K. Abu-Shandi, R. Thomann, H. Manyar, C. Hardacre and C. Janiak, *Chem. Eur. J.*, 2010, **16**, 3849-3858.